



A method for quantitative analysis of biofilm thickness variability
by Ricardo Murga

A thesis submitted in partial fulfillment of the requirements for the degree of Master of Science in
Environmental Engineering
Montana State University
© Copyright by Ricardo Murga (1994)

Abstract:

This thesis presents work done on developing an experimental method for measurement of biofilm thickness. This method involves embedding the biofilm, cross-sectioning it, and applying image analysis and mathematical techniques to reconstruct biofilm thickness profiles in order to characterize biofilm thickness variation. Quantitative data as well as qualitative observations obtained from *Pseudomonas aeruginosa*, *Klebsiella pneumoniae* and binary population biofilms revealed that the three biofilm systems are distinct and heterogeneous in their structure. Statistical analysis of biofilm thickness data showed that biofilm species composition influences structural characteristics. *P. aeruginosa*, *K. pneumoniae* and binary population biofilms appeared to have different mean thicknesses, different roughness values, and different spatial, distribution of biomass, voids and water channels. *P. aeruginosa* biofilms are relatively uniform and lack voids or water channels. They have an average thickness of 30 μm , and their roughness coefficient, Ra^* , ranges between 0.1 and 0.2. Different sizes and lengths of water channels were observed in *K. pneumoniae* biofilms, but the most distinctive characteristic was large bare areas along the substratum. *K. pneumoniae* biofilms are patchy and their thickness varies drastically, having a mean thickness that ranged between 8 μm to almost 300 μm . The roughness coefficient for *K. pneumoniae* biofilms was the highest of the three biofilms systems, ranging between 0.8 to 1.3. The binary population biofilm was also full of water channels and voids. The mean thickness ranged between 300 and 600 μm , but its roughness coefficient only ranged between 0.2 and 0.3. The different ranges for the roughness coefficient values suggested that differences in biofilm thickness variation could be used as a distinctive characteristic for categorizing biofilms.

A METHOD FOR QUANTITATIVE ANALYSIS OF BIOFILM
THICKNESS VARIABILITY

by
Ricardo Murga

A thesis submitted in partial fulfillment
of the requirements for the degree

of

Master of Science

in

Environmental Engineering

MONTANA STATE UNIVERSITY
Bozeman, Montana

April 1994

7378
m944

APPROVAL

of a thesis submitted by

Ricardo Murga

This thesis has been read by each member of the committee and has been found to be satisfactory regarding content, English usage, format, citations, bibliographic style, and consistency, and is ready for submission to the College of Graduate Studies.

4/27/94
Date

Philip A. Stewart
Chairperson, Graduate Committee

Approved for the Major Department

27 April 1994
Date

Shedice E. Lang
Head, Major Department

Approved for the College of Graduate Studies

5/4/94
Date

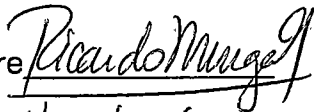
R. L. Brown
Graduate Dean

STATEMENT OF PERMISSION TO USE

In presenting this thesis in partial fulfillment of the requirements for a master's degree at Montana State University, I agree that the Library shall make it available to borrowers under rules of the Library.

If I have indicated my intention to copyright this thesis by including a copyright notice page, copying is allowable only for scholarly purposes, consistent with "fair use" as prescribed in the U.S. Copyright Law. Requests for permission for extended quotation from or reproduction of this thesis in whole or in parts may be granted only by the copyright holder.

Signature



Date

4/27/94

ACKNOWLEDGEMENTS

First I would like to express my gratitude to my academic and research advisor Dr. Phil Stewart. He has provided the support, guidance, and encouragement which have enabled me to accomplish this goal. I also thank my committee members, Dr. Warren Jones for his counsel and assistance during my first semester at MSU, and Dr. Zbigniew Lewandowski for his assistance.

I would like to acknowledge Gayle Callis for the many hours of work and for her advice on further developing biofilm cryoembedding. I would also like to acknowledge Don Daly for his advice and help on the use of statistical tools.

The staff and fellow graduate students at the Center for Biofilms Engineering have been very helpful to me, and have made my stay at the ERC very pleasant. I would like to especially thank for their help Gary, Dirk, Brian, Diane, Peg, Jamie, Paul, and Marty. Many thanks also for their help and friendship to Jason, Xiaoming, Philip, Sam, Mary, Nick, and specially Rohini.

I would like to acknowledge with love and gratitude the support and encouragement of my wife, Jennifer.

My special thanks to Bill Characklis for the existence of the Center, for his great example and vision.

My research activities have been sponsored by the National Science Foundation and the Associates of the Center; my thanks to them.

Most important of all I thank my God for His grace and love for me.

TABLE OF CONTENTS

	Page
LIST OF TABLES	vii
LIST OF FIGURES	viii
ABSTRACT	xi
INTRODUCTION	1
The Problem	1
Goal and Objectives	3
LITERATURE REVIEW	4
Evidence of Biofilm Structural Heterogeneity	4
METHOD DEVELOPMENT	10
MATERIALS, EXPERIMENTAL SYSTEMS AND METHODS	11
Bacterial Characteristics	11
Reactor Design	11
Reactor Start-up	16
Sampling	16
Biofilm Cryoembedding	18
Cryosectioning	19
Fixation and Staining of Biofilm Cross-sections	21
Image Analysis	22
Statistical Methods	23
RESULTS	27
DISCUSSION	64
Biofilm Thickness Measurements	64
Statistical Analysis	66
Biofilm Heterogeneity	68
SUMMARY AND CONCLUSIONS	74
RECOMMENDATIONS FOR FUTURE RESEARCH	77
REFERENCES	79

APPENDICES	86
APPENDIX A	87
Particle Sizing Using Image Analysis Techniques	87
Vernier Measurements	92
Coulter Counter Measurements	95
APPENDIX B	101
Optical Measurements	101
Biofilm Embedding	103
APPENDIX C	109
S-PLUS Program	109

LIST OF TABLES

Table		Page
1.	References for evidence of heterogeneity	5
2.	Medium composition	15
3.	Phosphate buffer composition	15
4.	Coulter Counter aperture tube data	99

LIST OF FIGURES

Figure		Page
1.	Annular reactor schematic	12
2.	Cryoembedding schematic	20
3.	Photomicrographs of the substratum after biofilm remov	32
4.	Photomicrographs of <i>P. aeruginosa</i> biofilm cross-section	33
5.	Photomicrographs of <i>K. pneumoniae</i> biofilm cross-section ...	34
6.	Photomicrographs of binary population biofilm cross-section ..	35
7.	<i>P. aeruginosa</i> biofilm profiles from three different random locations on the slide (a, b and c)	36
8.	<i>K. pneumoniae</i> biofilm profiles from three different random locations on the slide (a, b and c)	37
9.	Binary population biofilm profiles from three different random locations on the slide (a, b and c)	38
10.	<i>P. aeruginosa</i> biofilm thickness distributions from profiles on figures 7a through 7c	39
11.	<i>K. aeruginosa</i> biofilm thickness distributions from profiles on figures 8a through 8c	40
12.	Binary population biofilm thickness distributions from profiles on figures 9a through 9c	41
13.	Variogram curves from <i>P. aeruginosa</i> biofilm profiles on figures 7a through 7c	42
14.	Variogram curves from <i>K. pneumoniae</i> biofilm profiles on figures 8a through 8c	43
15.	Variogram curves from binary population biofilm profiles on figures 9a through 9c	44
16.	Values of Ra* (roughness coefficient) for <i>P. aeruginosa</i> , <i>K.</i> <i>pneumoniae</i> , and binary population biofilms	45

17.	2-day old binary population biofilm profiles from four different random locations on the slide	46
18.	4-day old binary population biofilm profiles from four different random locations on the slide	47
19.	6-day old binary population biofilm profiles from three different random locations on the slide	48
20.	8-day old binary population biofilm profiles from four different random locations on the slide	49
21.	Binary population biofilm thickness distributions from profiles on figures 17a through 17d	50
22.	Binary population biofilm thickness distributions from profiles on figures 18a through 18d	51
23.	Binary population biofilm thickness distributions from profiles on figures 19a through 19c	52
24.	Binary population biofilm thickness distributions from profiles on figures 20a through 20c	53
25.	Variogram curves from profiles on figures 17a through 17d . . .	54
26.	Variogram curves from profiles on figures 18a through 18d . . .	55
27.	Variogram curves from profiles on figures 19a through 19c . . .	56
28.	Variogram curves from profiles on figures 20a through 20c . . .	57
29.	Ra* values from biofilm profiles on figures 17a through 20c . . .	58
30.	Mean biofilm thickness from biofilm profiles on figures 17a through 20c	59
31.	Biofilm density for binary population biofilm 2, 4, 6, 8 days old .	60
32.	Individual cells and multicellular aggregates observed in the effluent of a <i>P. aeruginosa</i> biofilm reactor	61
33.	Multicellular aggregates observed in the effluent of a <i>K. pneumoniae</i> biofilm reactor	62

34.	Individual cells and multicellular aggregates observed in the effluent of a binary population biofilm reactor	63
35.	Relationship between Ra^* and variogram distance for <i>P. aeruginosa</i> , <i>K. pneumoniae</i> and binary biofilms	71
36.	Photomicrographs of undefined mixed population biofilm cross-section	72
37.	Photomicrographs of binary population biofilm cross-section grown with continuous supply of $CaCO_3$ and kaolin	73
38.	Particle area distribution of detached <i>P. aeruginosa</i> multicellular aggregates from days 1 through 4	89
39.	Particle area distribution of detached <i>P. aeruginosa</i> multicellular aggregates collected on hours 1 through 4 of day 5	90
40.	Particle area distribution of detached <i>P. aeruginosa</i> multicellular aggregates collected on hours 5 through 8 of day 5	91
41.	Polar Planimeter	93
42.	Image Analysis and planimeter results comparison	96
43.	Planimeter results from measuring square and circular shapes	97
44.	Method for measuring wet biofilm thickness with an optical microscope	102
45.	<i>P. aeruginosa</i> and <i>K. pneumoniae</i> biofilm thickness profiles	106
46.	Undefined mixed population biofilm thickness profile	108

ABSTRACT

This thesis presents work done on developing an experimental method for measurement of biofilm thickness. This method involves embedding the biofilm, cross-sectioning it, and applying image analysis and mathematical techniques to reconstruct biofilm thickness profiles in order to characterize biofilm thickness variation. Quantitative data as well as qualitative observations obtained from *Pseudomonas aeruginosa*, *Klebsiella pneumoniae* and binary population biofilms revealed that the three biofilm systems are distinct and heterogeneous in their structure. Statistical analysis of biofilm thickness data showed that biofilm species composition influences structural characteristics. *P. aeruginosa*, *K. pneumoniae* and binary population biofilms appeared to have different mean thicknesses, different roughness values, and different spatial distribution of biomass, voids and water channels. *P. aeruginosa* biofilms are relatively uniform and lack voids or water channels. They have an average thickness of 30 μm , and their roughness coefficient, Ra^* , ranges between 0.1 and 0.2. Different sizes and lengths of water channels were observed in *K. pneumoniae* biofilms, but the most distinctive characteristic was large bare areas along the substratum. *K. pneumoniae* biofilms are patchy and their thickness varies drastically, having a mean thickness that ranged between 8 μm to almost 300 μm . The roughness coefficient for *K. pneumoniae* biofilms was the highest of the three biofilms systems, ranging between 0.8 to 1.3. The binary population biofilm was also full of water channels and voids. The mean thickness ranged between 300 and 600 μm , but its roughness coefficient only ranged between 0.2 and 0.3. The different ranges for the roughness coefficient values suggested that differences in biofilm thickness variation could be used as a distinctive characteristic for categorizing biofilms.

INTRODUCTION

The Problem

Microbial cells attach firmly to almost any surface submerged in an aquatic environment. The immobilized cells grow, reproduce, and produce extracellular polymers which help them form a complex matrix that provides structure to the biomass accumulation termed a *biofilm* (Characklis and Marshall, 1990). The adhesion to surfaces provides considerable advantages for bacteria within the biofilm. The biofilm matrix provides protection from antimicrobial agents, as well as facilitating the exchange of nutrients and genetic material due to close proximity of cells. While bacteria benefit from their close association with the surface, the physical presence of the biofilm compromises the function of the surface, reducing the efficiency of equipment in industry. This damage to the surface is referred to as biofouling. Some of the problems stemming from biofouling are summarized in the following paragraph.

Microbially induced corrosion (MIC) is initiated when clusters of bacteria form a patchy biofilm. These clusters establish microscale chemical gradients around the surface and thereby create both anodic and cathodic sites (Lee and Characklis, 1993., Geesey and Bremer, 1992., Videla and Characklis, 1992., Bremer and Geesey, 1991., Characklis et al. 1991, Geesey, 1990., Jelley et al., 1989., Characklis, 1989). Increase of fluid-frictional resistance in industrial

pipes results from the increase in biofilm thickness and roughness (Characklis, Zilver and Turkhia, 1981., Characklis and Turkhia, 1981., Picologlou et al., 1980., Kirkpatrick et al. 1980., Characklis, Zilver and Picologlou, 1978).

Increase of heat transfer resistance results from the accretion of biomass and inorganic sediments (Turakhia and Characklis, 1984., Mussalli and Characklis, 1984., Characklis et al. 1984, 1983., Zilver et al., 1982., Characklis Nimmons and Picologlou, 1981., Characklis, Zilver and Turakhia, 1981). Bacterial colonization of a variety of medical implants and devices results in persistent infections (Costerton, 1982., Marrie et al., 1982., Marrie and Costerton, 1983., Marrie and Costerton, 1984). Detachment of microbial aggregates into the bulk liquid degrades products in the paper manufacturing and water distribution processes (Nix, et al. 1992., Block, 1992., Jung, et al. 1990., McFeters, 1990., van der Wende, et al. 1989., LeChevallier, et al. 1988., Camper, et al. 1986).

Biofilm development and activity is the result of several physical, chemical and biological rate processes. Such processes include transport of cells to the substratum, adsorption of cells onto the substratum, growth and other metabolic processes within the biofilm, and detachment of portions of the biofilm. These processes are influenced by the biofilm structure and the properties of the environment around the biofilm. Surface roughness, for example, significantly influences transport rates and microbial attachment for several reasons including the following: 1) increased convective mass transport near the surface, 2) shelter from shear forces for small particles, and 3)

increased surface area for attachment (Characklis, W.G., 1981). Surface roughness is one of the many aspects that reflect the structural heterogeneity of the biofilm matrix. This structural heterogeneity should therefore be studied and quantitatively described in order to better understand, predict and solve the problems caused by biofouling. Obtaining quantitative information on surface roughness and structural heterogeneity remains a challenge to biofilm researchers.

Goal and Objectives

The long term goal of this research is to understand how biofilm structural heterogeneity impacts biofilm function. The broad objective of this thesis was to develop experimental methods and apply mathematical techniques to characterize biofilm thickness variation. The specific objectives were: 1) to develop an experimental method suitable for measurement of biofilm thickness profiles, 2) to construct 1-dimensional thickness profiles of steady state pure culture biofilms of *P. aeruginosa*, *K. pneumoniae*, and the binary population combination, 3) to calculate a roughness index (R_a^*) and to perform a spatial correlation analysis for each profile, 4) to obtain photomicrographs of particles in the effluent of pure culture and binary population biofilm reactors, 5) to document temporal changes in biofilm thickness characteristics during development of binary population biofilms by obtaining biofilm thickness profiles, R_a^* values, and spatial correlation analyses in time series.

LITERATURE REVIEW

Evidence of Biofilm Structural Heterogeneity

Recent publications provide evidence of structural heterogeneity in biofilms. Table 1 shows a few examples of the types of evidence described in publications from the last decade alone. Several techniques have been used to qualitatively describe biofilm structure including light microscopy, atomic force microscopy (AFM), scanning electron microscopy (SEM), transmission electron microscopy (TEM), confocal scanning laser microscopy (CSLM), and Fourier transmission infrared spectroscopy (FTIR). The systems in which these observations were made range from laboratory reactors to medical and industrial systems.

Many factors may contribute to the structural heterogeneity of biofilms such as the uneven distribution of microbial species, the presence of different shapes of bacteria buried in amorphous extracellular polymers that constitute the biofilm matrix, nitrogen bubble formation in some cases, shear and hydrodynamic forces, deposits of sediments, and encrustations on pipe walls. All these contribute to different forms of structural heterogeneity in biofilms due to the disruption of the microbial matrix and biomass detachment (sometimes leaving entire bare areas), helping to the formation of patchy biofilms. Most heterogeneous biofilms have water channels, pores, microtowers, ridges, and large variations in biofilm thickness and surface roughness.

Table 1. References for evidence of heterogeneity.

Author	Ref	Microorganism	Reactor Design	Evidence
Allen et al, 1980.	1	Mixed population.	Wat. dist. system	Electron micrographs revealed a hard but porous surface.
Bremer et al, 1992.	7	CCI#8 bacterium.	Copper coupons submerged in flasks with culture medium.	Atomic Force Microscopy (AFM) showed biofilm "several cells thick in places, distributed heterogeneously over coupon surface with considerable variation in surface contour.
Bryers, 1991.	9	<i>P. putida</i> .	Annular reactor.	Observed sloughing events due to nitrogen bubble formation that lead to disruption of the microbial matrix.
Bryers and Characklis, 1981.	10	Undefined mixed population from sewage.	Tubular reactor system running as CSTR	Microscopically, biofilms appeared as discrete fibers randomly distributed, 1.5 to 1500 μm long.
Capdeville et al, 1990.	12	Heterotrophes.	Annular reactor	SEM and photographs showed observations of thickness profile and top view of rough, filamentous and patchy surface.
Christensen et al, 1988.	24	Denitrifying biofilm from wastewater.	Annular reactor	Pictures show heterogeneity in biofilm accumulation due to nitrogen bubble formation.

Table 1 (cont.)

Eighmy et al, 1983.	29	Undefined biofilm from wastewater.	Inert substratum and supporting structure suitable for submersion in wastewater, bacterial adhesion and subsequent examination by TEM and SEM.	SEM and TEM micrographs showed filamentous non-smooth surface.
Gujer, 1987.	34		A model of segregation of biomass in biofilms.	Describes a biofilm as an inhomogeneous microbial matrix due to uneven distributions of microbial species.
Hamoda and Abd-el-bary, 1987.	35	Mixed culture from activated sludge.	Aerated submerged fixed-film (ASFF) bioreactor.	Microscopic observation of spongy biofilms with thickness of up to 2.3 mm.
Harremoes et al, 1980.	37	Denitrifying biofilm.	Annular reactor.	Extreme heterogeneity in biofilms due to nitrogen bubbles formation that detached big particles of biofilm leaving large bare sections of the wall visible.
Howell and Atkinson, 1976.	38		Trickling filter biofilm model.	Computer output showed film thickness profiles to have a varied irregular pattern.

Table 1 (cont.)

Huang et al, 1985.	39	Undefined mixed population from primary effluent from sewage treatment plant.	Annular reactor.	Microscopic observations showed biofilm texture that was loose and porous.
Kugaprasatham et al, 1992.	44	Nitrifying biofilm.	Cylindrical PVC reactors.	Photographic observations of patchy and filamentous biofilm where surface was not smooth.
Lawrence, J.R. et al, 1991.	45	<i>P. fluorescens</i> , <i>P.aeruginosa</i> , <i>Vibrio</i> <i>parahaemolyticus</i>	Gyratory shaker.	Highly hydrated biofilms, open structures 73 to 98% EPS and space. Also, significant channeling and porosity of the biofilm were observed.
LeChevallier et al, 1987.	46	Mixed population, bacteria, fungi, protozoa, yeasts, etc.	Distribution systems	SEM showed biomass attached to pipe walls in a heterogenous pattern determined by shear-forces, deposits of sediment, encrustations and tubercles on pipe wall surface.
Mack et al, 1975.	49	Mixed population, bacteria and algae.	Trickling filters.	SEM showed rough uneven surfaces.
Nickel and Costerton, 1992.	56	Klebsiella species and Enterococcus faecalis bacteriuria.	Foley catheter.	SEM depicted thick heterogenous multispecies biofilm.

2

Table 1 (cont.)

Picologlou et al, 1980.	59	Undefined mixed population from wastewater inoculum.	Tubular fouling reactor (TFR).	Fluid friction measurements indicate hydrodynamic roughness.
Robinson et al, 1984.	60	Methanogens.	Anaerobic fixed-bed reactor.	SEM showed volcano-like structures opening to the interior - 500 μm in diameter - overall surface was rough and uneven.
Rogers and Keevil, 1992.	61	Inoculum from outbreak of Legionnaires' disease.	Coupons of glass or polybutylene pipe sections suspended in two-stage chemostat model of a water distribution system.	Basal biofilm layer was approximately 5 μm with taller stacks exceeding 100 μm in height.
Siebel and Characklis, 1991.	63	<i>P. aeruginosa</i> , <i>K. pneumoniae</i> and binary of P. and K.	Annular reactor.	Nomarsky microscopic pictures showed P. biofilms to be somewhat smooth, K. biofilms to be clusters with bare spots in between, and the binary biofilm to be patchy with microtowers.
Siegrist and Gujer, 1985.	64	Heterotrophic biofilm.	Rotating biological contactor.	Filamentous and porous structured biofilm.

Table 1 (cont.)

Stewart, 1992.	66		Mathematical model of biofilm detachment.	Model incorporates the discrete nature of the detachment process and therefore the variations in biofilm thickness, patchiness and roughness.
Stewart et al, 1993.	67	<i>P. aeruginosa</i> biofilms.	Annular reactor.	Optical method and image analysis showed evidence of heterogeneity in both surface roughness and size of the detached biomass in the effluent.
Switzenbaum and Eimstad, 1987.	68	Methanogens.	Anaerobic fixed-film reactors (AF, AFB and UASB).	SEM showed dense and thin films with rough uneven surfaces, channels and ridges.

METHOD DEVELOPMENT

The objective of this thesis came about from the desire to quantify one of the qualities that describe the structure of biofilms. Prior to pursuing a method for measuring biofilm thickness variability, a research goal was to develop a method for measuring the size of the biomass particles that detach from biofilms. Three methods were pursued, none of which were successful. Appendix A explains these methods.

Developing a method for measuring biofilm thickness also required much effort. Two different methods were pursued before trying the cryoembedding of biofilm, which worked the best. The first two methods are explained in Appendix B.

MATERIALS, EXPERIMENTAL SYSTEMS AND METHODS

Bacterial Characteristics

Pseudomonas aeruginosa and *Klebsiella pneumoniae* were used to grow mono and binary population biofilms. *Pseudomonas aeruginosa* is a Gram-negative rod shaped (approximately 0.5 to 1.0 μm by 1.5 to 4 μm) aerobic chemoorganotroph. It is motile by means of a single polar flagellum. (Brock, 1974). *Pseudomonas aeruginosa* is an obligate aerobe, although in some cases nitrate (NO_3^-) can be used as an alternate electron acceptor. The optimum temperature for growth is 37°C, although growth occurs from below 4°C to 43°C.

Klebsiella pneumoniae is a Gram-negative straight rod shaped (0.3 - 1.0 μm by 1.0 - 6.0 μm) non-motile chemoorganotroph. This organism is a facultative anaerobe, having both respiratory and fermentative metabolic pathways. Its optimum temperature for growth is 35°C, although growth can occur from 10°C to 44°C (Bergey's, 1984).

Reactor Design

A continuous flow annular reactor (Figure 1) was used to grow biofilm. The reactor design has several characteristics which make it versatile for biofilm research (Peyton, 1992). It consists of two polycarbonate cylinders, a stationary outer cylinder and a co-axial rotating inner cylinder. The inner

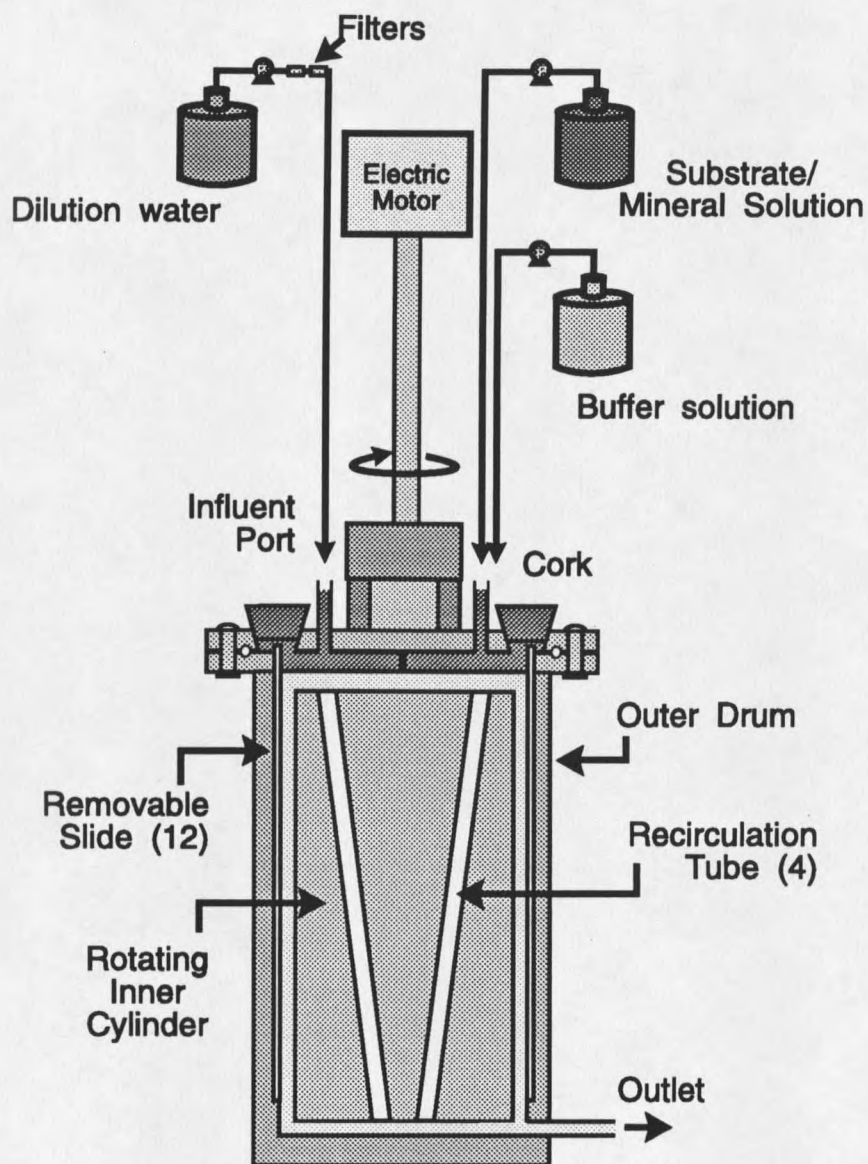


Figure 1. Annular reactor schematic.

cylinder has four vertical draft tubes positioned at angles so that the rotation of the inner cylinder pumps the fluid through the tubes providing vertical mixing. The reactor can thus be considered to be well-mixed (Characklis & Marshall, 1990). The inside wall of the outer cylinder, with an area of $676 \times 10^{-4} \text{ m}^2$ upon which biofilm can grow, has vertical grooves that allow twelve removable slides for sampling of biofilm. The slides, each with an area of $33 \times 10^{-4} \text{ m}^2$, can be removed through the top of the reactor through rubber-stoppered holes. Fluid shear stress in the reactor is dependent on the rotational speed of the inner cylinder. The outer cylinder undergoes a uniform shear stress since the gap between cylinders is constant throughout the height of the reactor (Drury, 1992). Because the shear stress is constant and the reactor is completely mixed, it is commonly assumed that the biofilm growing on the walls of the outer cylinder is relatively uniform, so that a biofilm specimen collected from any of the twelve slides is a representative sample. Also, because the annular reactor is completely mixed, the effluent from the annular reactor is a representative sample of the bulk fluid.

Three separate streams were added to the annular reactor, producing a cumulative flow rate of $19.2 \times 10^{-4} \text{ m}^3 \text{ h}^{-1}$ (32 ml/min), and a hydraulic retention time of 0.34 h. At this retention time, suspended bacteria are quickly washed away from the reactor and their activity can be neglected. The three streams were substrate ($6 \times 10^{-5} \text{ m}^3 \text{ h}^{-1}$, or 1 ml min^{-1}), phosphate buffer ($6 \times 10^{-5} \text{ m}^3 \text{ h}^{-1}$, or 1 ml min^{-1}), and dilution water ($0.0018 \text{ m}^3 \text{ h}^{-1}$, or 30 ml min^{-1}). Tables 3 and 4

show the composition of substrate and phosphate buffer, respectively. Flow rates were measured with in-line flow meters (Gilmont Instruments Co., Nos. 11 and 12). Peristaltic pumps (Masterflex #7553-30, Cole-Parmer Instruments Co., with pump heads 7021-20 and 7518-00) were used to supply the substrate, buffer solution, and dilution water.

Dilution water was RO water (Culligan Automatic Water Conditioner, Culligan USA Division) filtered using an ultrapure water system (NANOpure Mod. No. D4741, Barnstead/Thermolyne). The solution water was aerated to ensure oxygen saturation before it was supplied to the annular reactor.

Sterilization of the dilution water was obtained by filtering through two 0.2 μm capsule filters (Gelman Sciences, Inc., #12122) in series.

Nutrient (not including glucose) and phosphate buffer solutions were prepared in 10 L containers and autoclaved at 121°C for 6 hours. Glucose was added to the container by injecting 10 ml of concentrated glucose solution through a septum. The glucose solution was filter-sterilized through a 0.2 μm filter (Sterile Acrodisk, Gelman Sciences, Product No. 4129) at the time of addition. All experiments were conducted at room temperature.

TABLE 2

SUBSTRATE (in 10 L carboy)

Glucose	6.4516 g (add after autoclave)
KNO ₃	4.352 g
MgSO ₄	0.3225 g
CaCO ₃	0.3225 g
Trace minerals:	(in stock, add 10 ml)
(HOCOCH ₂) ₃ N	0.0645 g
(NH ₄) ₆ Mo ₇ O ₂₄ · 4H ₂ O	0.000451 g
ZnSO ₄ · 7H ₂ O	0.0485 g
MnSO ₄ · H ₂ O	0.003677 g
CuSO ₄ · 5H ₂ O	0.000903 g
NaB ₄ O ₇ · 10H ₂ O	0.000451 g
Co(NO ₃) ₂ · H ₂ O	0.000741 g
FeSO ₄ · 7H ₂ O	0.05129 g
<i>Flow rate = 1 ml/min</i>	

TABLE 3

BUFFER (in 10 L carboy)

KH ₂ PO ₄	65.6 g
Na ₂ HPO ₄	136.32 g
<i>Flow rate = 1 ml/min</i>	

Reactor Start-up

The reactor system, Masterflex 6411-15 tubing (Cole-Parmer Instrument Co.), and SS slides (316L) were washed with Micro-soap solution (Cole-Parmer Instrument Co., model 8790-10).

The reactor assembly (including the twelve slides, connecting tubing, flowmeters, flow breaks, and dilution water filters) was autoclaved for 25 min at 121°C. All open tube ends were covered with aluminum foil. Connections were made to the substrate and phosphate buffer containers through sterile glass tubing. The reactor was filled with substrate, buffer solution, and dilution water in the right proportion using the peristaltic pumps. Rotation of the inner cylinder was initiated and the reactor ran abiotically for a couple of hours, after which time all pumps were stopped. One ml frozen stock culture (10^8 cells/ml) of each bacterial species was allowed to melt from -70°C to room temperature. The reactor was then inoculated with the thawed bacterial stock by injecting it through a septum and allowing it to grow in batch mode for 24 hours. After this incubation period, influent flows were started again.

Sampling

Effluent for microscopic evidence of detached particles.

Eighteen ml of the reactor effluent were collected and fixed with 2 ml of 2% formaldehyde. 0.6 ml of the fixed effluent was stained with 0.6 ml of acridine orange (AO) for 7 min, and then filtered through a 0.2 μ m Nuclepore

polycarbonate filtration membrane (Costar Corporation). The membrane was placed on a microscope slide in order to be photographed using a 35mm camera (Olympus C-35AD-2) mounted on the microscope (Olympus BH-2).

Effluent plated for viability and contamination.

Every day approximately 10 ml of the reactor effluent were collected and homogenized for 1 min using a tissumizer (Tekmar Co., Typ. SDT 1810, and TR-10 power controller). Several dilutions of the homogenized effluent were plated daily for viable count. The drop plate method (Miles and Misra, 1938) and an electronic digital pipette (EDP2, RAINI Instrument Co. Inc.) were used.

Biofilm sampled for determination of total bacterial number.

The slides were removed from the annular reactor and the biofilm scraped into 100 ml of phosphate buffer solution and homogenized for 5 min. 9 ml of the homogenized cells were fixed with 1 ml of 2% formaldehyde. A Nuclepore polycarbonate membrane (pore size of 0.2 μm and 25mm diameter) was placed on a cell free glass Millipore filter apparatus, and rinsed with cell free water. 0.05 ml of the sample was added along with 0.1 ml of AO and allowed to stain for 10 min. The dye solution was removed with vacuum (about 13KPA) and the filter rinsed again with about 1 ml of water. The filter was placed on the top of a drop of oil (R.P. Cargille Laboratories Inc., non drying immersion oil type FF) on a microscope slide and covered with another drop of oil and a glass cover slip. The total number of bacteria on the filter was calculated using a microscope and the microscope eye-piece grid. For better

statistical results 10 or more grid fields were observed each time for a total of 400 or more cells counted.

Biofilm Cryoembedding

Cryoembedding is a technique adapted from tissue histopathology.

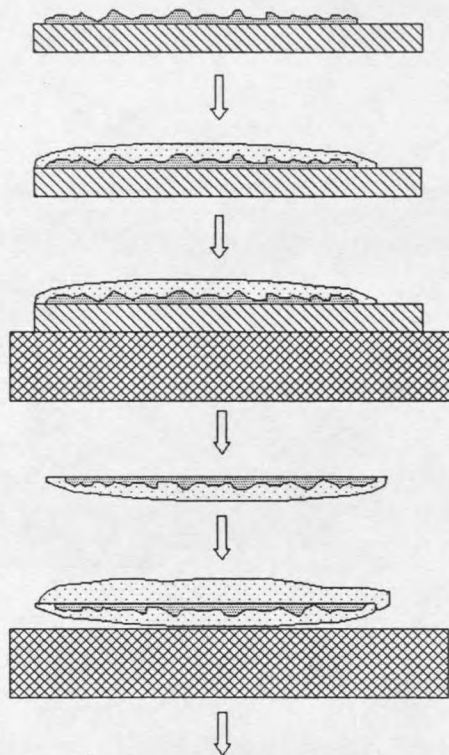
Using a commercial tissue embedding medium, cryoembedding preserves the physical structure of the biofilm (Yu, P. et al).

Cryoembedding the biofilm requires ideal instant freezing upon addition of the embedding agent (Tissue-Tek OCT [optimum cutting temperature] compound, Miles Inc.). Nearly instant freezing could only be achieved by placing the biofilm sample on dry ice (CO_2), and allowing conduction through the slide to reach the biofilm and freeze it. Initial attempts were unsuccessful. The slide was removed from the reactor and placed on top of the dry ice. The biofilm was immediately covered with a thick layer of the embedding medium and allowed to freeze. The biofilm was separated from the substratum by gently bending the slide to remove the frozen biofilm. The frozen specimen was then turned over and a thick layer of embedding agent was added to embed the side that was previously attached to the substratum, letting it overflow on every edge. Everything was done carefully at room temperature, but when the samples were cryosectioned the biomass shattered. After many experimental runs and wasted biofilm samples, the biofilms continued to shatter. The only possible reason was that ice crystals were being formed during the freezing and when the blade tried to cut the sections the ice crystals

shattered. Pouring the embedding agent first and then placing the slide on the dry ice was also tried and the same results were obtained. If indeed crystals were being formed during the embedding procedure, there were two possible sources: it could be that the embedding agent was not infiltrating the biofilm (OCT was not designed for infiltration) and the water voids and water channels were still full of water; or perhaps when the biofilm was removed from the substratum and a second layer of the embedding agent was added, condensation was occurring resulting in ice crystals entrapped between the two layers of embedding agent. Both possibilities were solved by letting the embedding agent sit for 5 to 10 minutes allowing it to displace as much water as possible from channels and voids before freezing. The embedded biofilm was then placed on dry ice and allowed to rapidly freeze until the whole specimen turned opaque white. After 5 more min the specimen (still attached to the slide) was wrapped in aluminum foil and stored at -70°C . See Figure 2 for cryoembedding steps.

Cryosectioning

Frozen sections were cut with a cryostat (Reichert-Jung Cryocut 1800, Leica) operated at -19°C . The frozen specimen from storage at -70°C was placed back on dry ice inside the cryostat to ensure a very low temperature and then separated from the substratum (slide) by gently bending the slide to remove the frozen biofilm. The frozen specimen was then turned over and



CRYOSECTIONING

A slide was removed from the Rotatorque, and the biofilm immediately covered with a thick layer of a cryoembedding agent (Tissue-Tek OCT [optimum cutting temperature] compound, Miles Inc.). The embedding agent was allowed to infiltrate the biofilm for 10 min. The embedded biofilm was then placed on dry ice and allowed to rapidly freeze until the whole specimen turned opaque white. The frozen specimen was then placed inside the cryostat for the rest of the procedure. The specimen was turned over, removed from the dry ice and allowed to equilibrate to -18°C for 10 min. A thick layer of embedding agent was added to embed the side that was previously attached to the substratum, letting it overflow on every edge. The sample was transferred back to dry ice (while still inside the cryostat) to rapidly freeze until opaque white. The specimen was then removed from the dry ice, and allowed to again reach thermal equilibrium inside the cryostat.

Figure 2. Cryoembedding schematic.

removed from the dry ice, but kept in the cryostat for 10 min to allow thermal equilibration. A thick layer of embedding agent was added to embed the side that was previously attached to the substratum, letting it overflow on every edge. The sample was transferred back to dry ice to rapidly freeze until opaque white. The specimen was then removed from the dry ice, and allowed to again reach thermal equilibrium inside the cryostat. A blade at room temperature was used to bisect small pieces of cryoembedded biofilm, 1 to 2 cm long. A small amount of embedding agent was poured onto a precooled (-19°C) specimen chuck and the small specimen pieces pressed onto the embedded medium. When the embedding agent solidified, the specimen sample was fixed on the chuck and ready for sectioning. The specimen was oriented perpendicular to a disposable microtome blade (#815, Reichert-Jung, Leica). Each 5 μm thick frozen cross section was collected on a glass slide (Superfrost Plus, Fisher Scientific) for fixation and staining.

Fixation and Staining of Biofilm Cross-sections

Sections on glass slides were dried overnight, fixed with 95% ethanol for 5 minutes, and air dried for 30 minutes. Sections were then stained in Gill II hematoxylin for 6 minutes and rinsed gently with running tap water for 2 minutes. Sections were blued in Scott's tap water substitute for 30 seconds, rinsed with running tap water for 2 minutes, dehydrated through 70% ETOH (1 change) for 1 min, 95% ETOH (2 changes) 1 minute each, 100 % ETOH

(2 changes) 1 minute each, xylene (2 changes), and finally coverslipped with permanent mounting media.

Image Analysis

American Innovision Videometric 150

The American Innovision Videometric 150 image analysis software (American Innovision Inc.) was used to capture and store photomicrographs of the biofilm cross-sections, using a American Innovision Inc. Color CCD, 1.5 LUX camera (Unit# 150) camera mounted onto a Olympus BH-2 microscope with transmitted light. First the objective settings and camera zoom settings had to be calibrated using an Olympus Object Micrometer (Scientific Instrument Co.) and color video monitor (Mod. No. PVM-1342Q, Sony Corporation).

Once captured, the images were converted to ".TIF" files and imported into another image analysis software, Mark (Harkin and Shope, 1993), for the measurement of biofilm thickness. For details see American Innovision Videometric 150 user's manual.

The Mark Image Analysis Software

The images retrieved into the Mark software were analyzed for biofilm thickness. Thickness was measured in the direction of the flow. Therefore, profiles were reconstructed showing the x-axis as distance along the substratum in the direction of the flow.

A description of the software calibration and procedure for analyzing

images follows. When Mark is initiated, a small window will appear with the only option "File." Enter "File" and another window will open with different options. Using the mouse, select the correct directory under "Directories," under "Files" select the correct filename, make sure the right filename shows in the "Selection" window, and enter "OK." A bigger window will now appear showing the image you retrieved. On the menu option "Enhance," select "Spread" (for a sharper black and white image). Under the menu option "Registration," select "Calibrate" and a window for the calibration method will appear. Select "Enter pixels per unit length," and enter "OK." The Calibrations units window will appear, select "Micron," and enter "OK." A request for the number of pixels per micron will appear. For the example of $10 \text{ Pix} = 9.77$, the number to be entered should be $10 \div 9.77$, or 1.0235415, followed by "Enter." A window for setting the grid spacing will appear, select "2" microns using the mouse, then enter "Done." Another window will appear requesting the name desired for the file that will contain the thickness measurements every $2 \mu\text{m}$ and the corresponding cumulative distance along the substratum. To terminate select "Close" under the main menu option "File."

Statistical Methods

The Mark Image Analysis System generated files which contained thickness of the biofilm versus the distance along the substratum. Thickness was measured every $2 \mu\text{m}$. These files were imported into the statistics

software S-PLUS (Statistical Sciences, Inc.) which was used to generate thickness profiles, Ra^* , and variogram curves for statistical analyses of the data. A hardcopy of the code used for the calculations can be found in Appendix C.

The first statistical analysis performed on the thickness data was to calculate a coefficient of surface roughness or thickness variability, Ra^* . This coefficient was suggested by the common and well accepted measure of surface roughness Ra , which measures the mean absolute deviation. Ra is defined as

$$Ra = \frac{1}{N} \sum_{i=1}^N |Lf_i - \overline{Lf}|$$

where Lf_i is each of the thickness measurements, overlined Lf is the mean thickness, and N is the number of thickness measurements. However, Ra was used to analyze biofilm thickness data and was found to be strongly correlated to the mean thickness. Therefore, in order to standardize Ra for different mean thickness values, Ra^* was derived as the ratio of Ra to mean thickness. Ra^* was defined as

$$Ra^* = \frac{1}{N} \sum_{i=1}^N \frac{|Lf_i - \overline{Lf}|}{\overline{Lf}}$$

Ra^* is an index of how much the thickness measurements deviate from the mean thickness.

The next statistical analysis performed on these thickness data was the spatial correlation analysis based on a variogram. The variogram is a measure

of the correlation (association) as a function of distance. If there is a strong association between two variables, then knowing one can do a great deal to predict the other. But when there is a weak association, information about one variable does not help much in estimating the other. Correlation is measured from a cloud of data points which are half the squared difference between two data points a set distance "d" apart along the substratum. The variogram function, denoted by the greek letter gamma, is a curve fit through the data points in the correlation cloud using non parametric regression. The variogram can also be estimated as

$$\gamma(d) = \frac{1}{2N} \sum_{(i,j) | d_{ij}=d} (Lf_i - Lf_j)^2$$

where (Lf_i, Lf_j) are all pairs of thickness measurements separated a distance "d," and N is the number of pairs. The spatial correlation between two data points is always a value between 0 and 1, expressed as $\rho(d)$ ($0 \leq \rho(d) \leq 1$), and it is an index of linear association between two data points a certain distance "d" apart. A correlation value of zero means no linear association between the two data points, while a correlation value of 1 represents the best linear association. Thus, conceptually, the variogram analysis can be expressed as

$$\gamma(d) = \sigma^2(1 - \rho(d))$$

where σ^2 is the total variation. As $\rho(d)$ ranges between 1 and zero, $\gamma(d)$ varies between zero and σ^2 . This range of values corresponds to the part of the

variogram curve that indicates best to no linear association between two thickness measurements. Therefore, the information provided by the variogram analysis can be obtained by finding the location where the slope of the variogram curve reaches zero ($\gamma(d) = \sigma^2$), and reading the corresponding value of distance. This is the distance at which two thickness measurements become uncorrelated. In other words, this is the minimum distance required between two thickness measurements in order for them to have no linear association.

More information on the variogram curve and coefficient of variation can be found in Isaaks et al (1989) and Freedman et al (1980).

RESULTS

An experimental method has been developed for measurement of biofilm thickness. This method involves embedding the biofilm, cross-sectioning it, and applying image analysis and mathematical techniques to recreate biofilm thickness profiles in order to characterize biofilm thickness variations. The procedure for cryoembedding and cryosectioning the biofilms is explained in detail in the "Materials, Experimental Systems and Methods" section of this thesis. A schematic of the embedding procedure is found in Figure 2. Photomicrographs of the slide were obtained (Figures 3a and 3b) in order to ensure that the biofilm was being removed thoroughly and not leaving layers of cells attached to the substratum. Figures 4 through 6 are photomicrographs of mature biofilm cross sections obtained from *P. aeruginosa* biofilm, *K. pneumonia* biofilm, and binary population biofilms respectively.

Thickness profile plots were created by using image analysis systems to measure thickness every 2 μm along the substratum for distances of a few thousand micrometers. These profiles, however, do not represent the structure of the biofilm. Thickness measurements do not distinguish between the dense biofilm matrix and water channels or voids. Each thickness measurement represents the distance between the substratum and the outermost cell, skipping over voids and channels. Three thickness profiles from a pure *P. aeruginosa* mature biofilm are shown in Figures 7a, 7b and 7c. The mean

thickness varied between 28 and 31 μm for these biofilms. Also apparent is a localized thickness variation where the maximum and minimum values of thickness never differed by more than 40 μm . Three different profiles from a pure *K. pneumoniae* mature biofilm are shown in Figures 8a, 8b and 8c. These profiles show the diverse structure and thickness variation of pure *K. pneumoniae* biofilms. The mean thickness ranged from 8 to 260 μm . Large areas of bare substratum can be observed which help classify pure *K. pneumoniae* biofilms as patchy. Three different profiles from a binary population mature biofilm are shown in Figures 9a, 9b and 9c. Binary population biofilms are distinct from the pure culture biofilms in that the mean thickness varied between 205 and 640 μm . All profiles were obtained from three random locations on the slide.

The thickness measurements shown on the profiles can be presented also as cumulative percentage plots. These plots show the percentage of thickness measurements that were equal to or less than the corresponding thickness shown in the x-axis. Figures 10a through 12c show the respective cumulative percentage plots of thickness for profiles on Figures 7a through 9c.

One of the statistical analysis performed on these thickness data was the spatial correlation analysis based on a variogram. The variogram is a measure of the correlation (association) as a function of distance. See statistical methods section of Materials and Methods for an explanation of this analysis. Figures 13a through 15c show the variograms corresponding to biofilm profiles

on Figures 7a through 9c. Notice that the correlation distances varied considerably even within the same species, see Figure 35. *P. aeruginosa* biofilms thickness measurements are independent at distances that range between 100 to 380 μm . The thickness measurements for *K. pneumoniae* biofilms are independent at a distance that varies between 500 and 4400 μm . And similarly, thickness measurements for binary population biofilms are independent at distances varying between 760 and 4800 μm .

Figure 16 shows the values of Ra^* for the biofilm profiles on Figures 7a through 9c. Notice that Ra^* values fall in three distinct ranges which correspond to the three distinct biofilms analyzed; 0.10 to 0.17 for *P. aeruginosa* biofilms, 0.83 to 1.33 for *K. pneumoniae* biofilms, and 0.21 to 0.30 for binary population biofilms. Both the variogram and Ra^* have proven to be useful statistical tools for describing the very distinct thickness profiles of the three different biofilm systems.

The next set of results (Figures 17a through 31) describe the changes in thickness variability for a binary population biofilm during the first eight days of its development. For this particular experiment, the biofilm was grown with the trace minerals listed on Table 3 and glucose as the only source of nutrients, KNO_3 , MgSO_4 , and CaCO_3 were not added to the substrate. Figures 17a 17b, 17c and 17d show profiles of the biofilm on day 2 from four random locations on the slide. These profiles show the initial patchy colonization of the substratum, with mean thickness values ranging from 2 to 4.3 μm . Figure 18

(a, b, c, and d) shows profiles from day 4. These profiles show a fully grown biofilm with a very rough surface. Mean thickness values varied between 28 and 161 μm . Figure 19 (a, b, and c) shows profiles from day 6, very similar to those from day 4, having mean thickness values varying between 97 and 117 μm . Finally, Figure 20 (a, b, and c) shows profiles from day 8, where surface roughness and thickness has diminished from those of previous days, having mean thickness values between 23 and 40 μm . Another way of visualizing the surface roughness is through cumulative percentage plots. Figures 21 (a, b, c, d), 31 (a, b, c, d), 32 (a, b, c), and 33 (a, b, c) correspond to the thickness distribution of profiles on Figures 17a through 20c. Figures 25 (a, b, c, d), 35 (a, b, c, d), 36 (a, b, c), and 37 (a, b, c) correspond to Figures 17a through 29c, and they show their variogram curves. These curves are very helpful in showing the distance along the substratum at which two thickness measurements become uncorrelated. Thickness measurements of the biofilms on day 2 are independent at a distance that varied between 190 and 450 μm . On day 4 the distance varied between 490 and 1600 μm . On day 6 this distance varied between 850 and 3900 μm , and on day 8 it varied between 320 and 2000 μm . Figure 29 shows the Ra^* values for the profiles from days 2, 4, 6, and 8. Ra^* values varied for each day, ranging between 1.12 and 1.4 on day 2, between 0.25 and 0.99 on day 4, between 0.23 and 0.93 on day 6, and between 0.76 and 0.98 on day 8. Figure 30 shows how the mean thickness from those profiles varied with time. Here we see that the values of thickness

were very consistent for days 2 and 8, but during the time at which surface roughness was maximum, they were hard to predict. Figure 31 shows the biofilm density, expressed as number of cells per meter cubed for days 2, 4, 6 and 8. Biofilm density varied between 3.6×10^{15} and 1.35×10^{17} cells/m³. For each type of biofilm, photomicrographs of the cellular aggregates found in the effluent of the reactor were obtained. Figures 32, 33 and 34 are photomicrographs of typical aggregates of cells collected from the effluent of the reactor. They picture aggregates detached from pure culture *Pseudomonas aeruginosa*, *Klebsiella pneumoniae*, and binary population biofilms, respectively. All the photographs collectively showed that in *P. aeruginosa* biofilm systems the main mechanism of detachment is erosion of individual cells. They also show that *K. pneumoniae* biofilm systems undergo detachment in the form of sloughing. Sloughing occurs when large multicellular aggregates detach from the biofilm surface sometimes leaving behind large areas of the substratum bare.

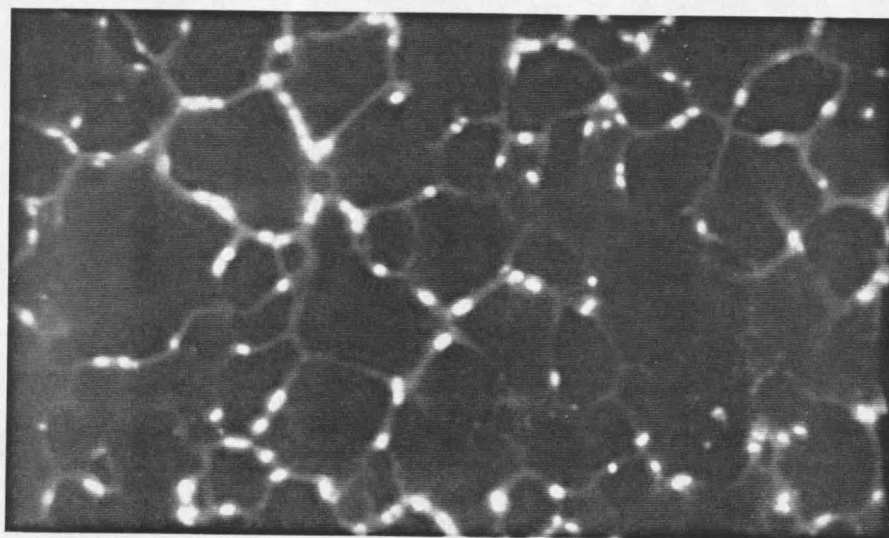
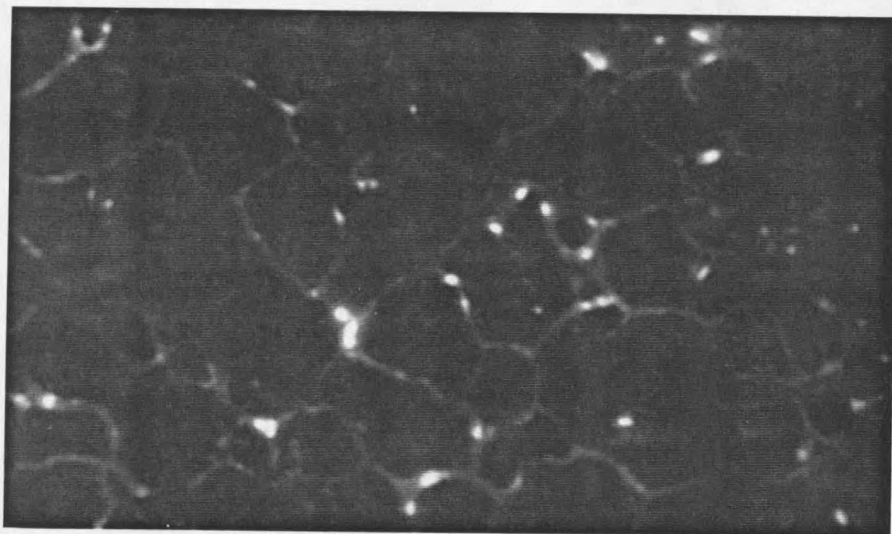


Figure 3. Photomicrographs of the substratum after biofilm removal. Small white dots are retained cells.

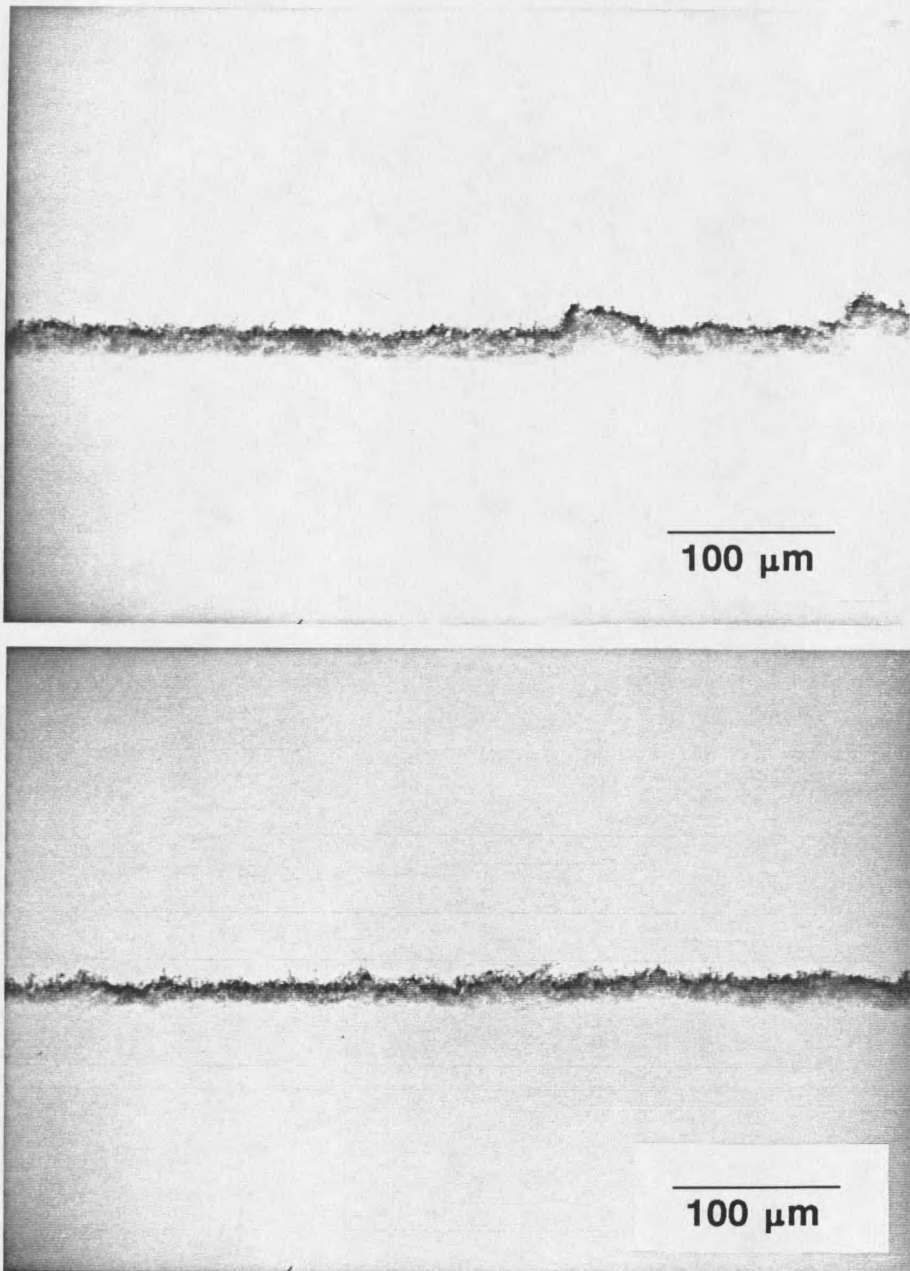


Figure 4. Photomicrograph of *P. aeruginosa* biofilm cross-section.

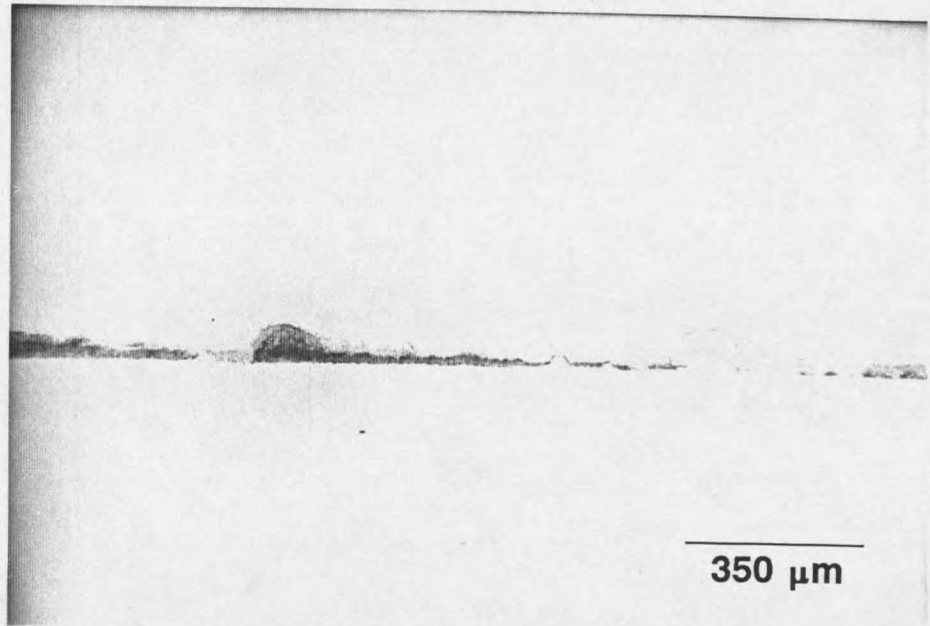
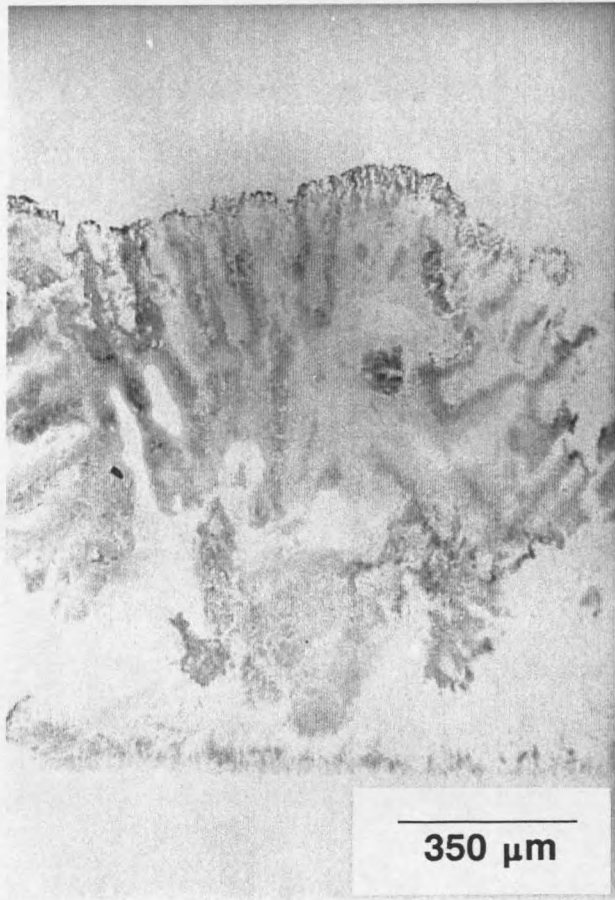


Figure 5. Photomicrograph of *K. pneumoniae* biofilm cross-section.

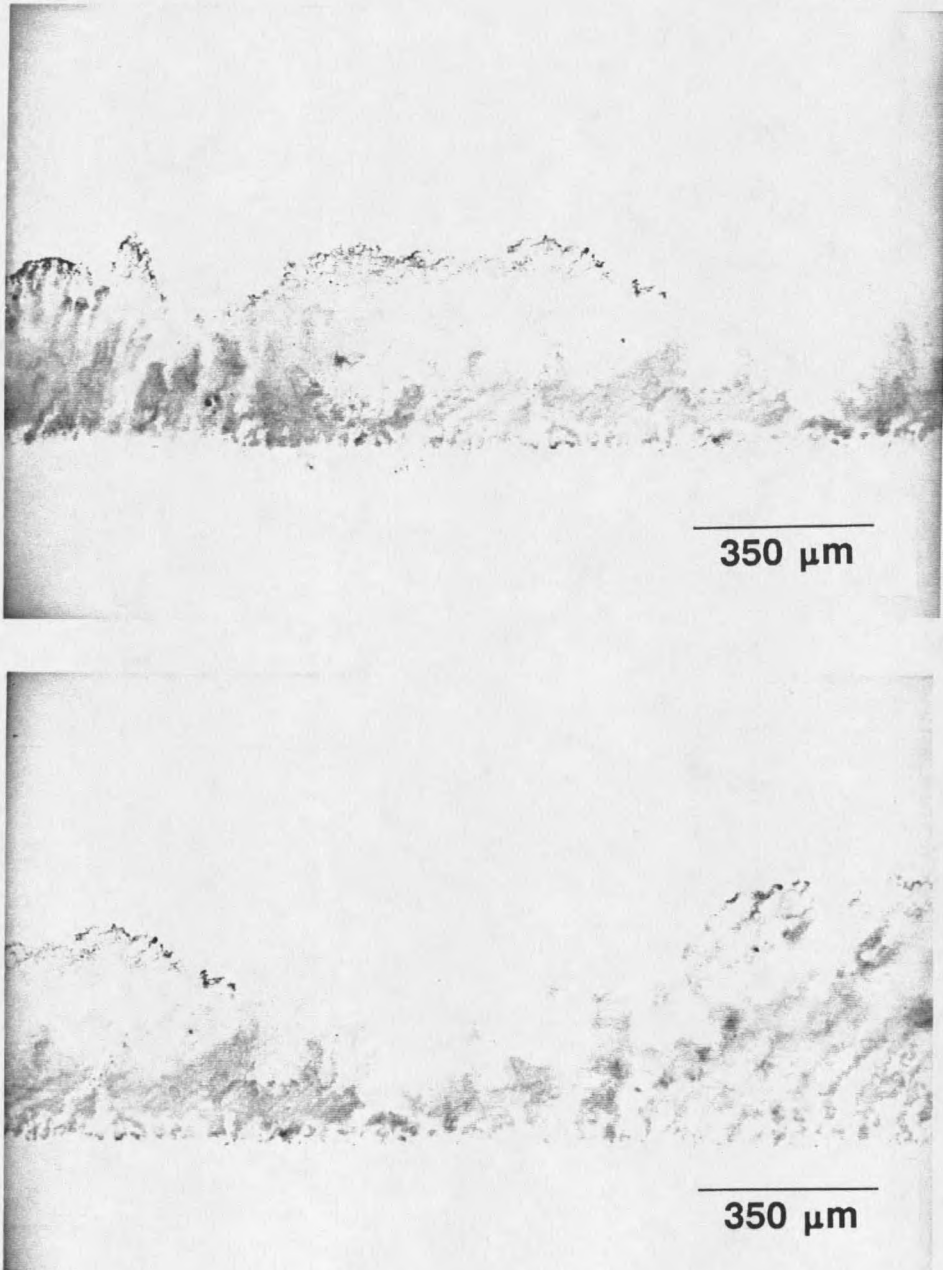


Figure 6. Photomicrograph of binary population biofilm cross-section.

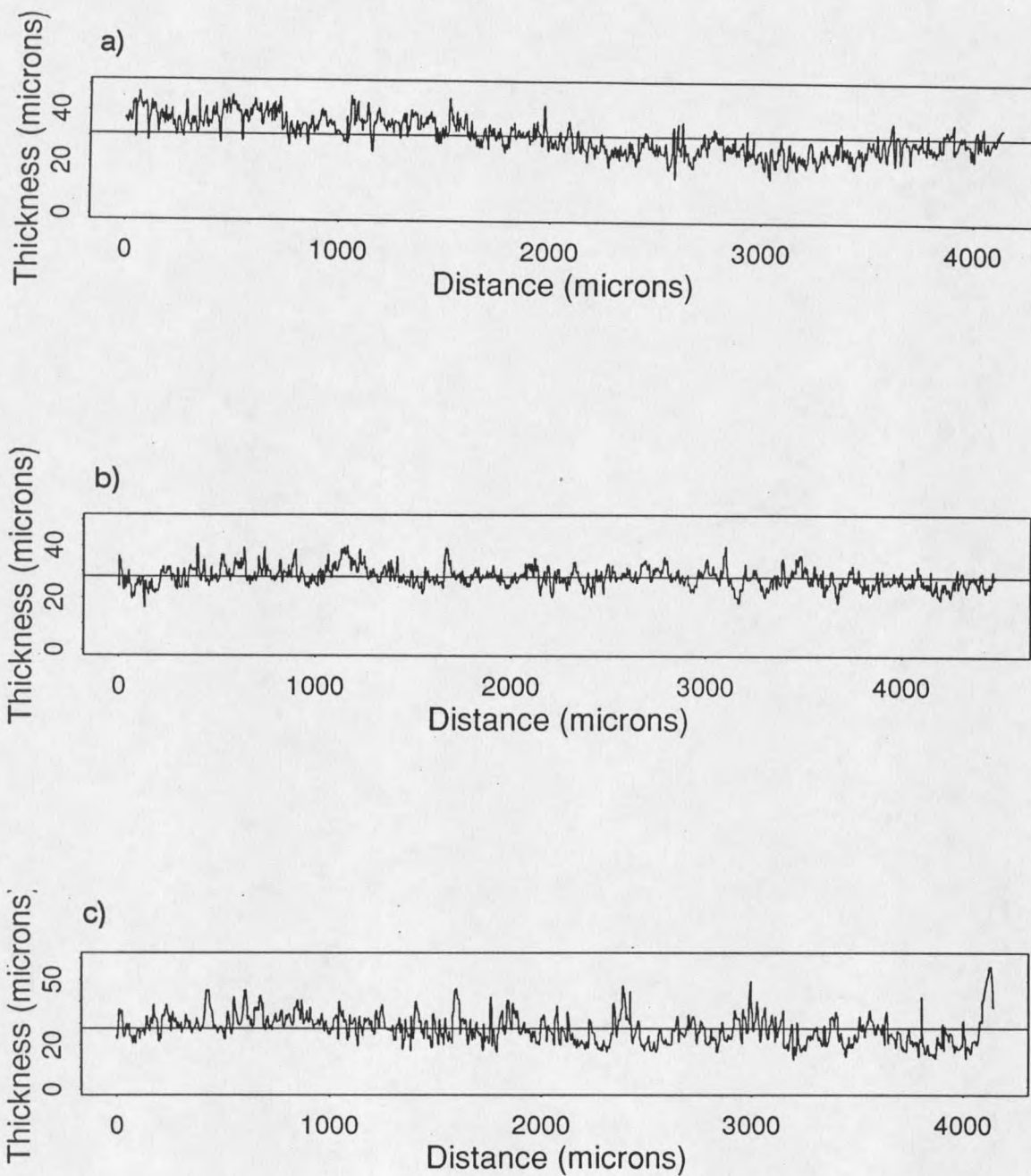


Figure 7. *P. aeruginosa* biofilm profiles a), b) and c) from three different random locations on the slide.

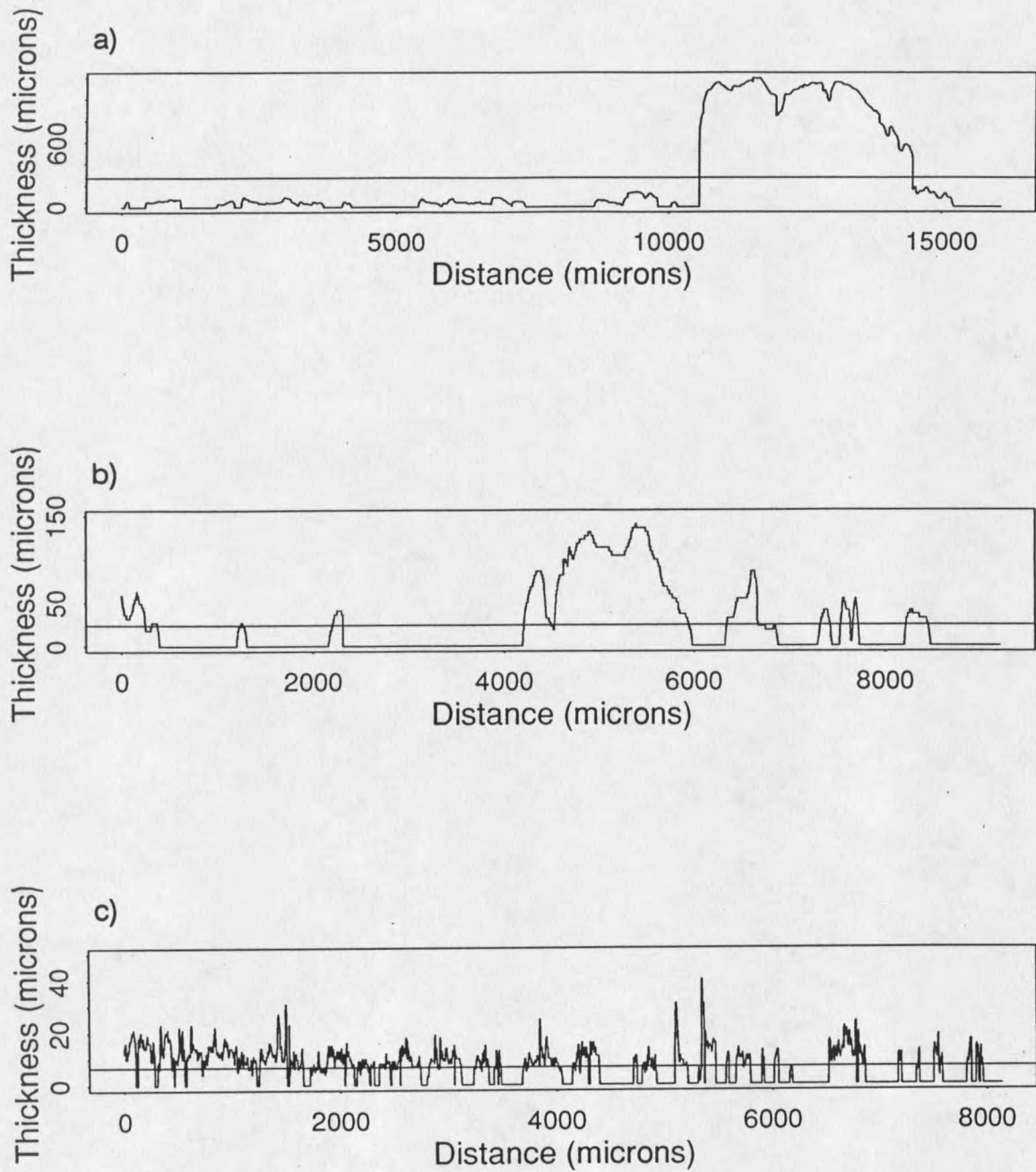


Figure 8. *K. pneumoniae* biofilm profiles a), b) and c) from three different random locations on the slide.

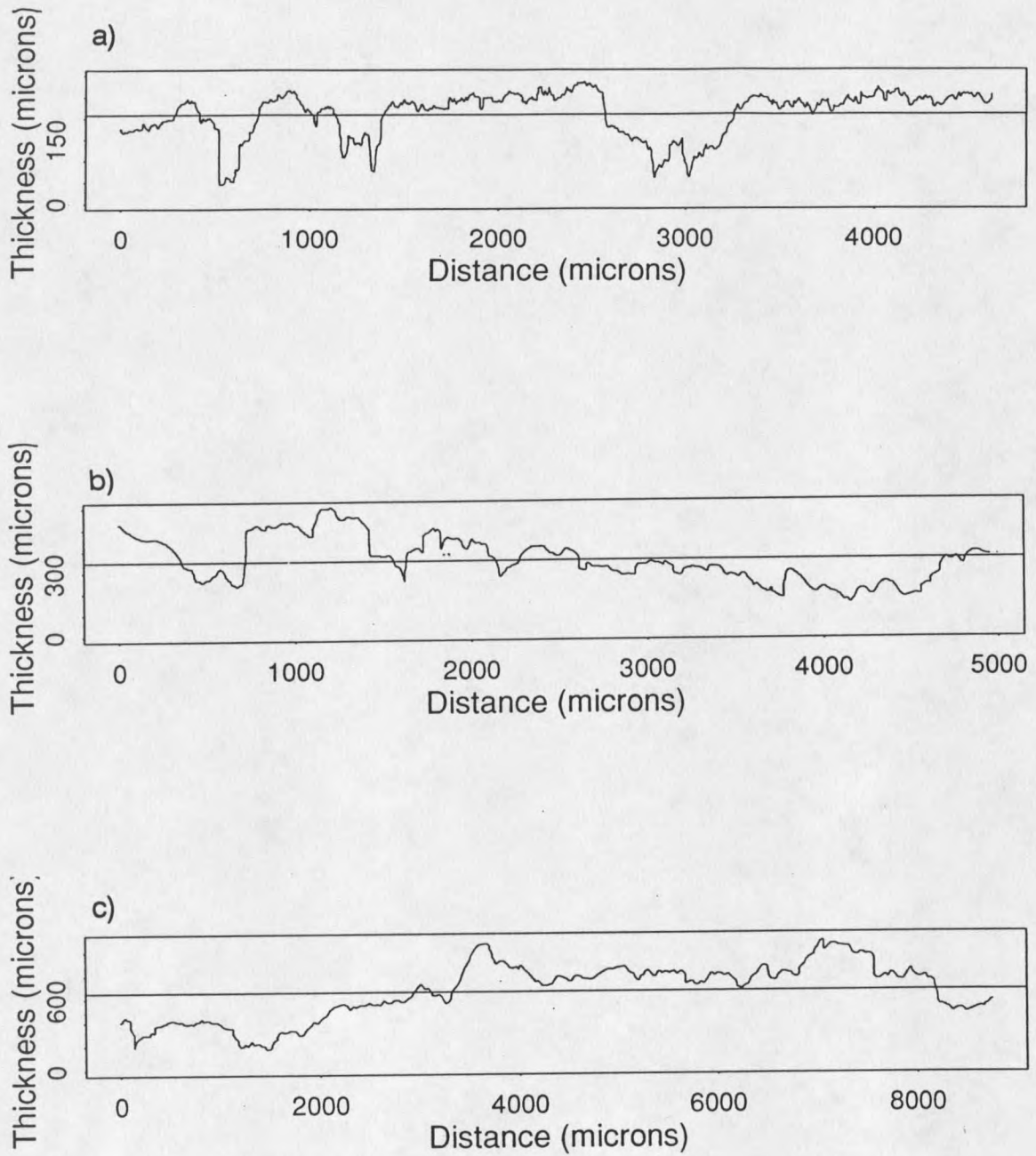


Figure 9. Binary population biofilm profiles a), b) and c) from three different random locations on the slide.

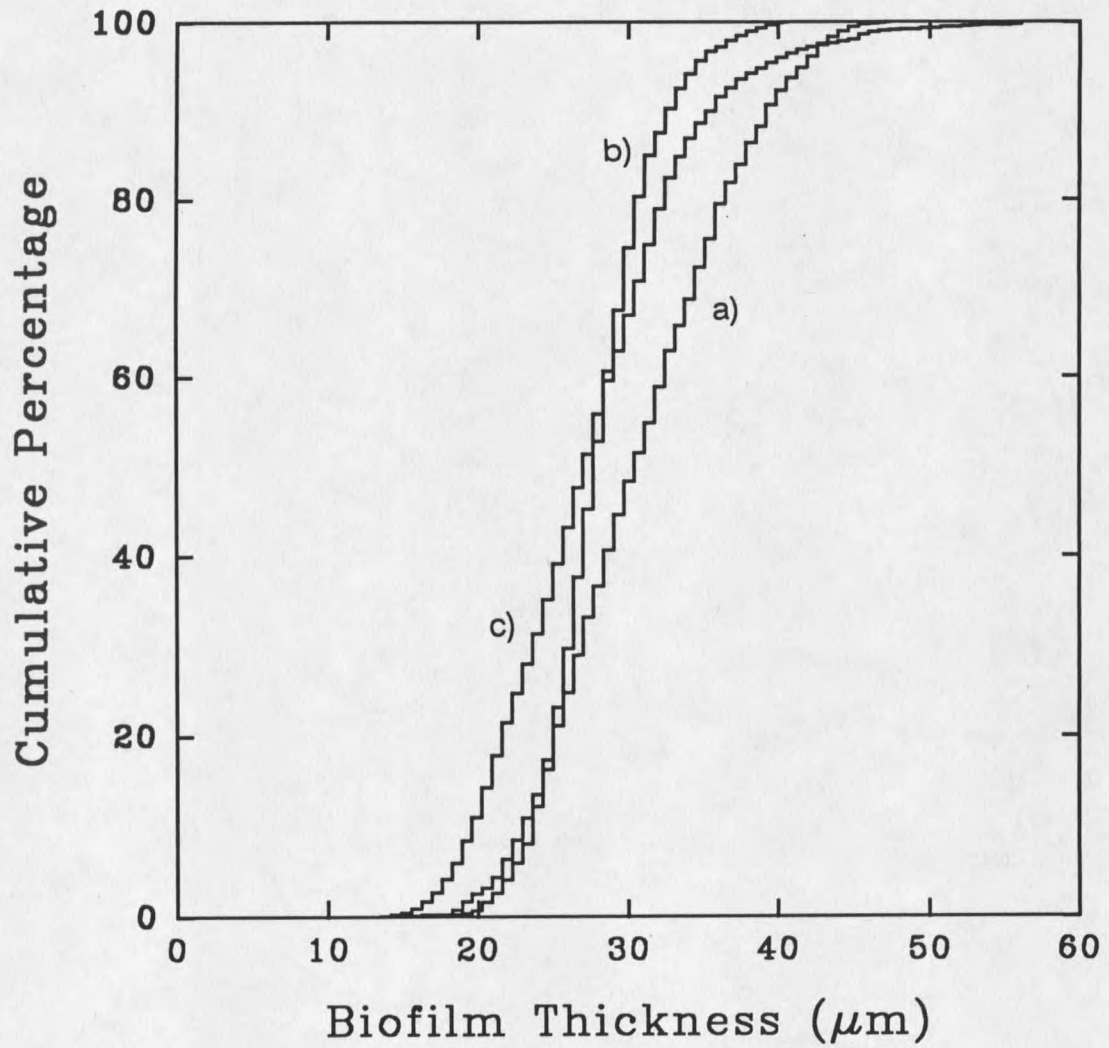


Figure 10. *P. aeruginosa* biofilm thickness distributions a), b) and c) from profiles on Figure 7a through 7c.

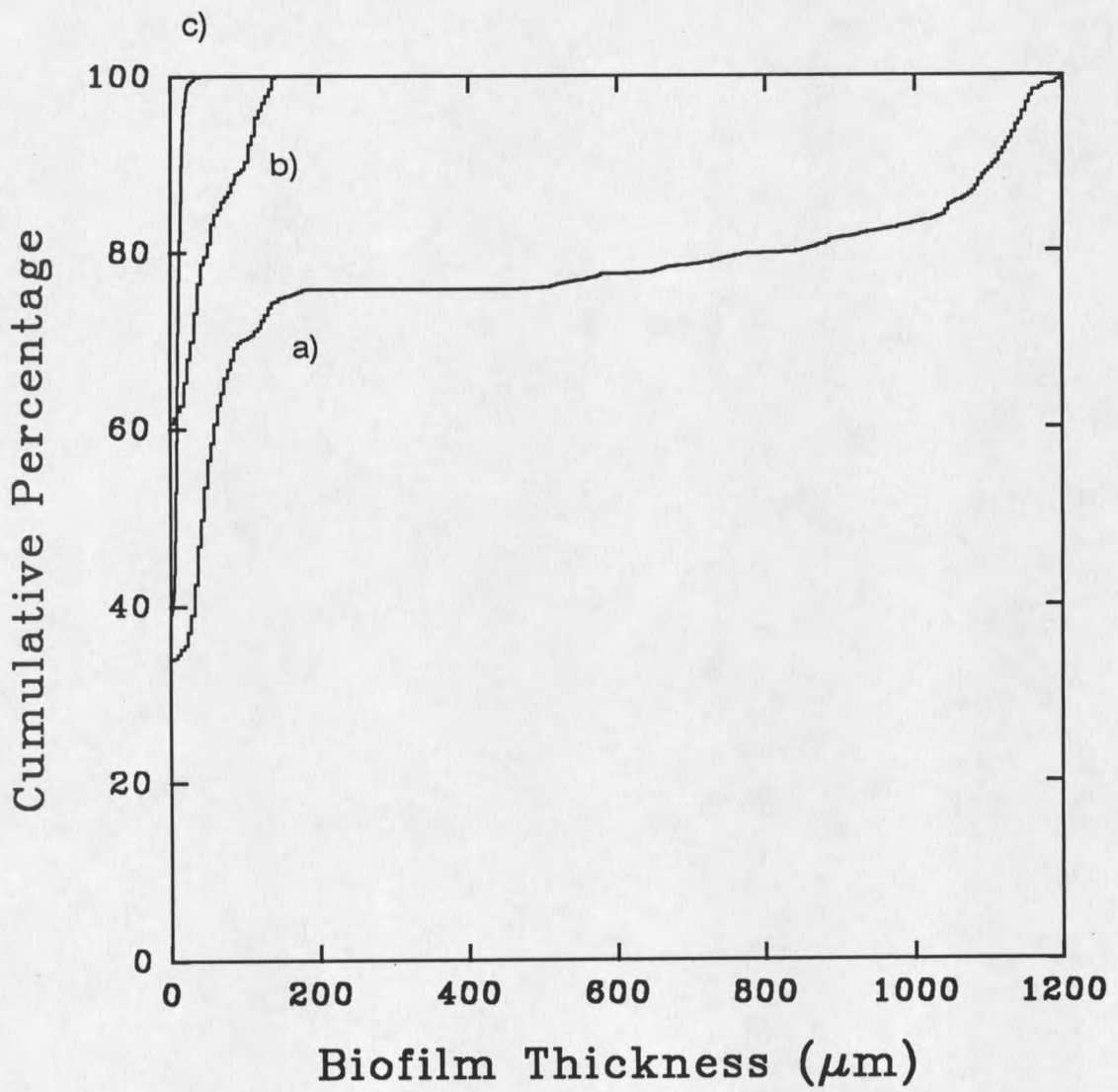


Figure 11. *K. pneumoniae* biofilm thickness distributions a), b) and c) from profiles on Figure 8a through 8c.

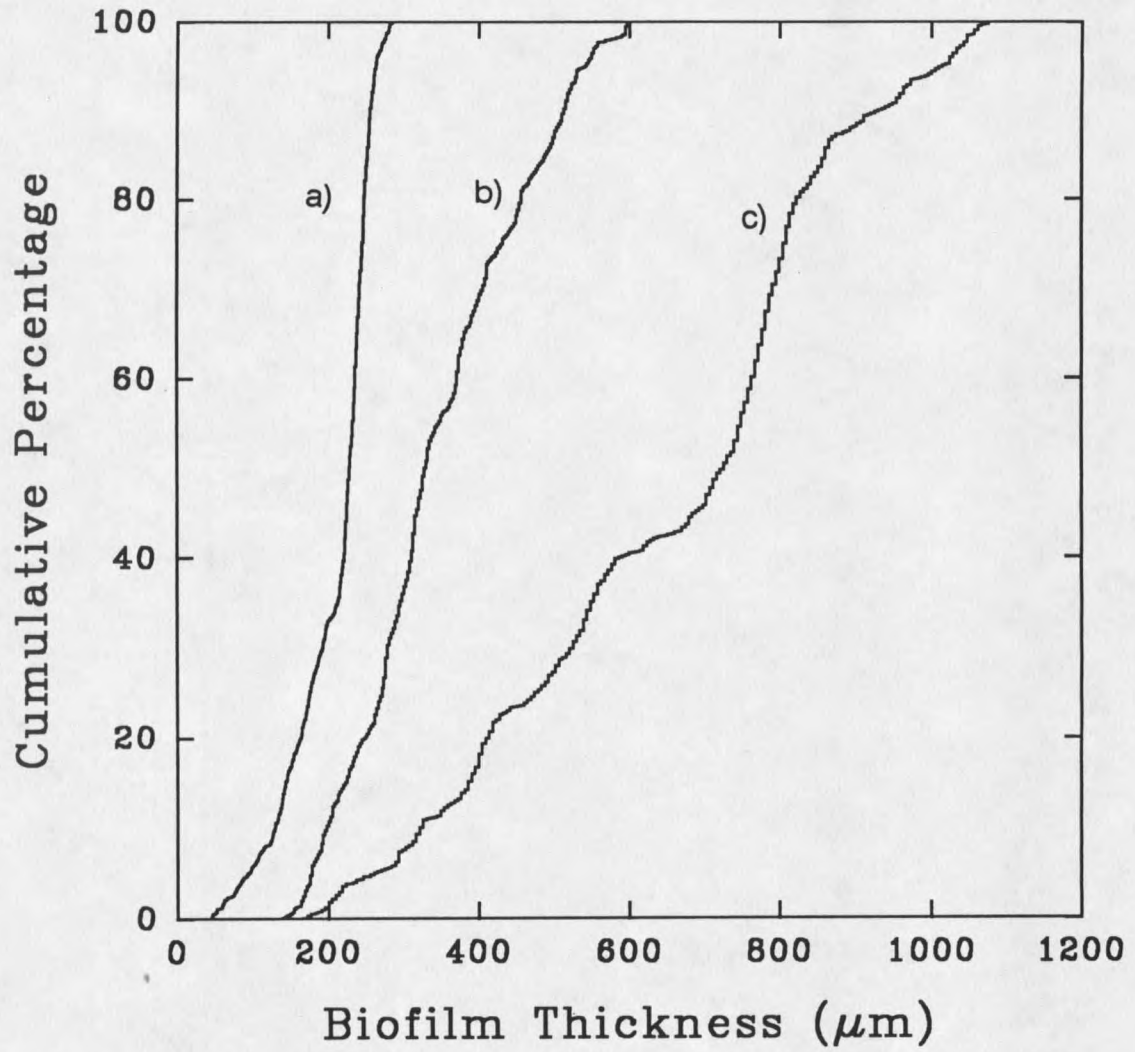


Figure 12. Binary population biofilm thickness distributions a), b) and c) from profiles on Figure 9a through 9c.

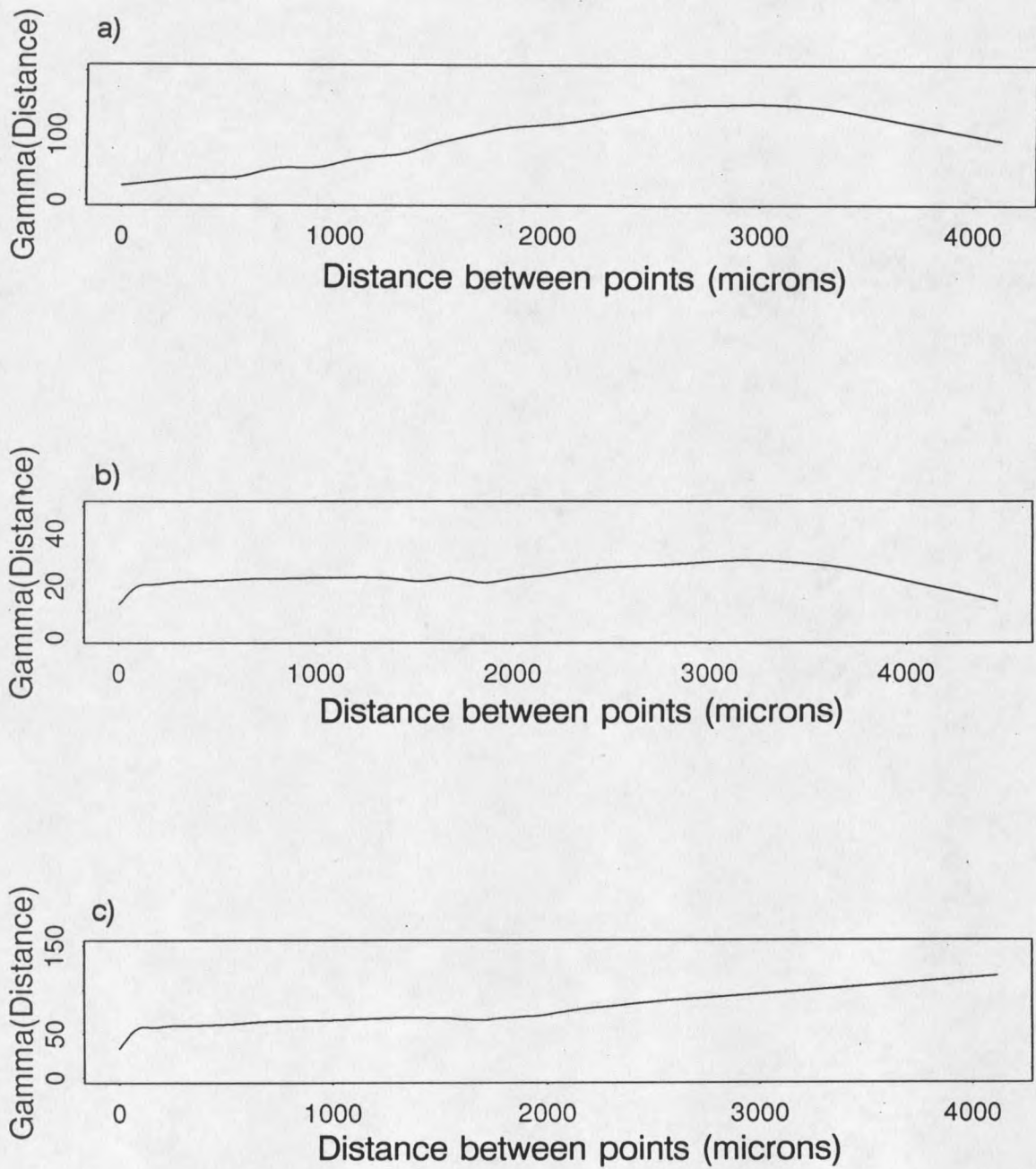


Figure 13. Variogram curves from *P. aeruginosa* biofilm profiles on Figure 7a through 7c.

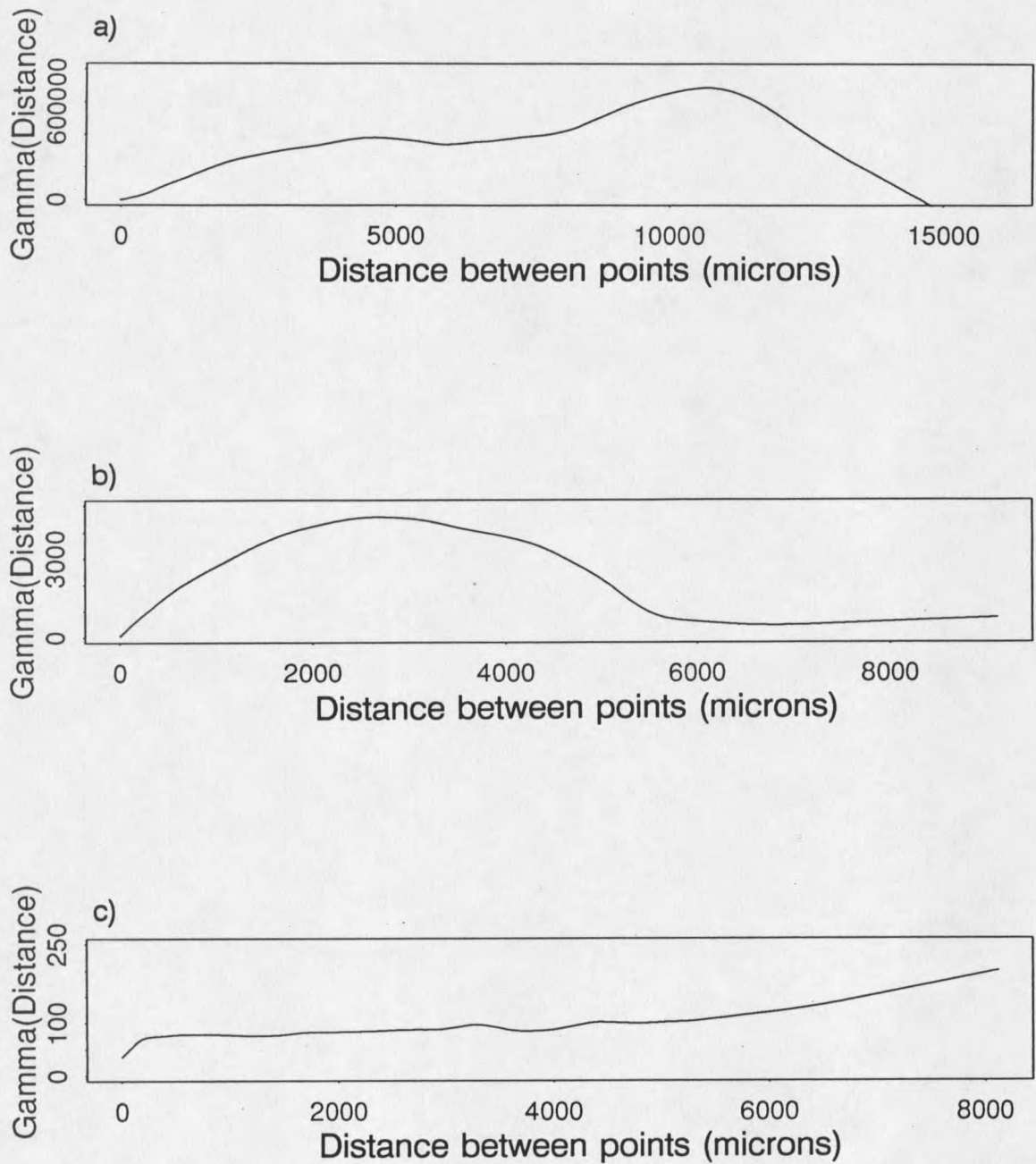


Figure 14. Variogram curves from *K. pneumoniae* biofilm profiles on Figure 8a through 8c.

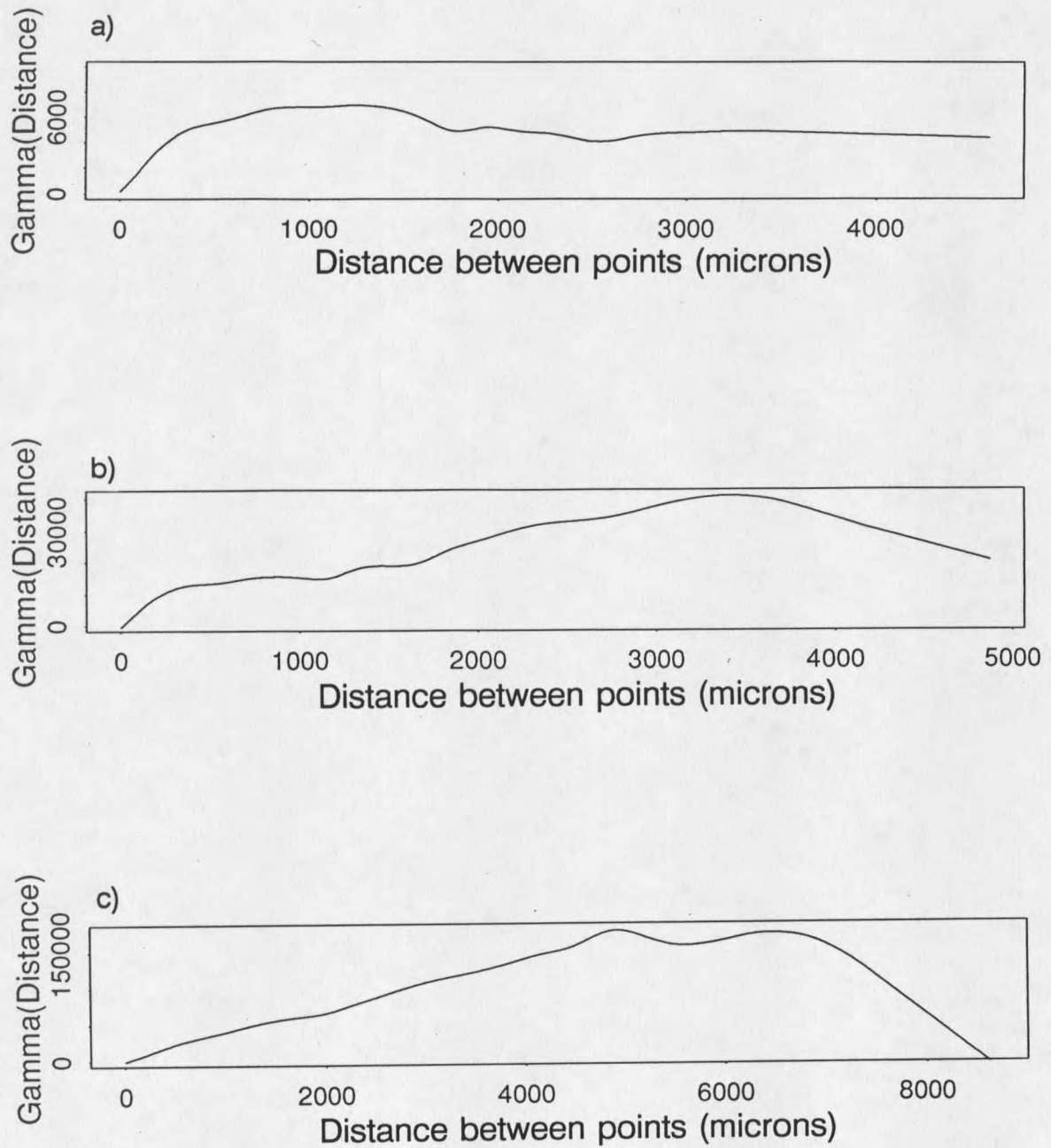


Figure 15. Variogram curves a), b) and c) from binary population biofilm profiles on Figure 9a through 9c.

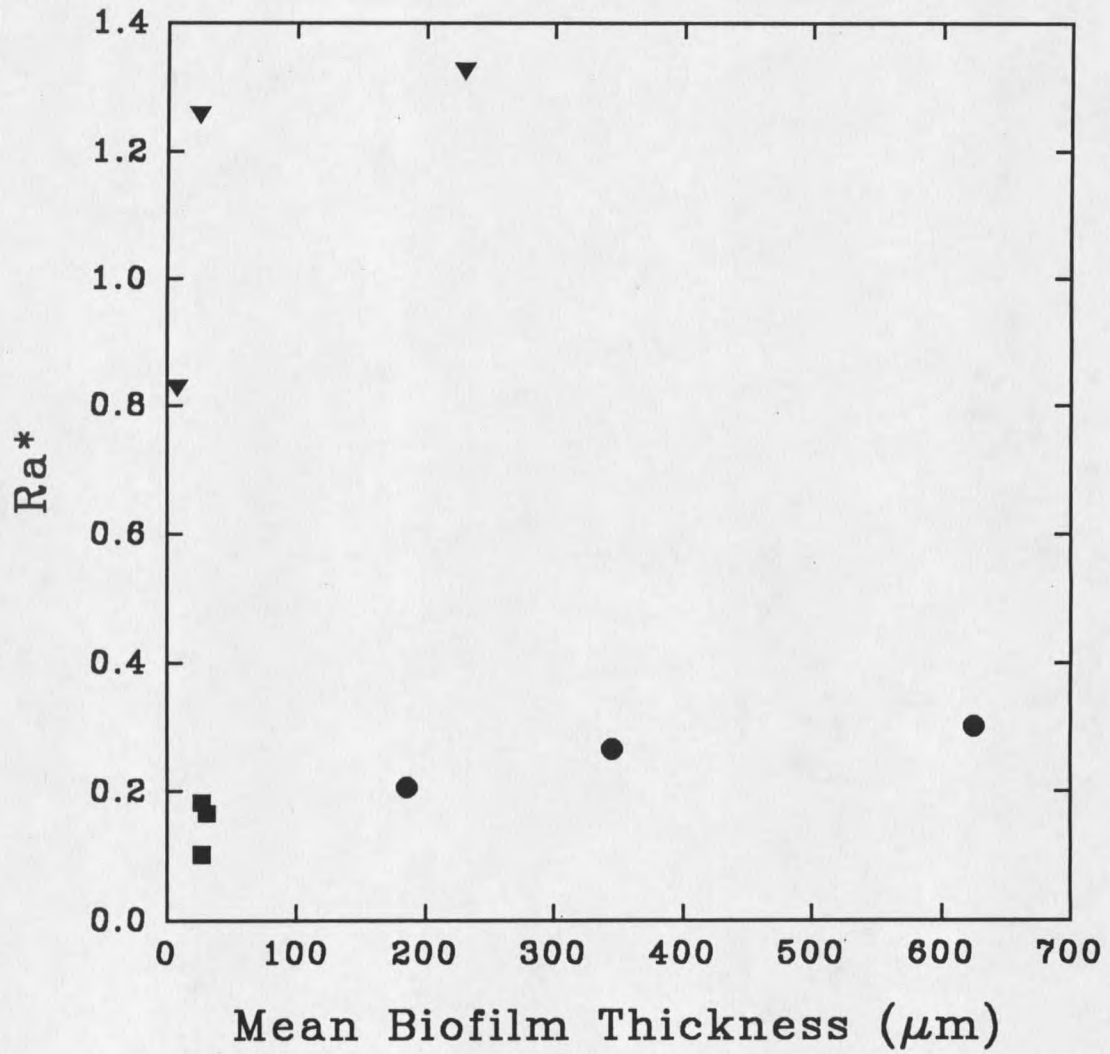


Figure 16. Values of Ra^* (roughness coefficient) for (■) *P. aeruginosa*, (▼) *K. pneumoniae*, and (●) binary population biofilms.

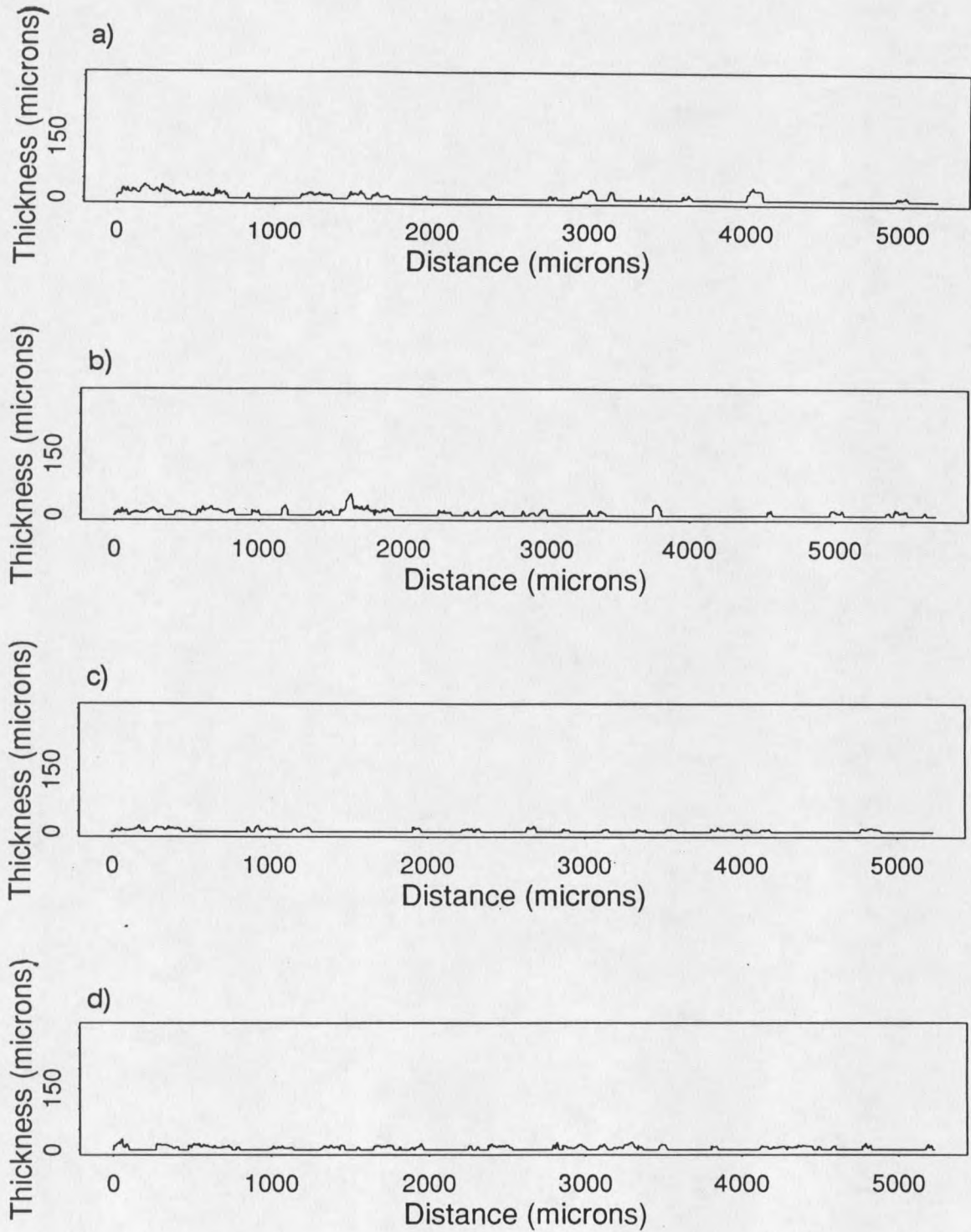


Figure 17. 2-day old binary population biofilm profiles a), b), c) and d) from different random locations on the slide.

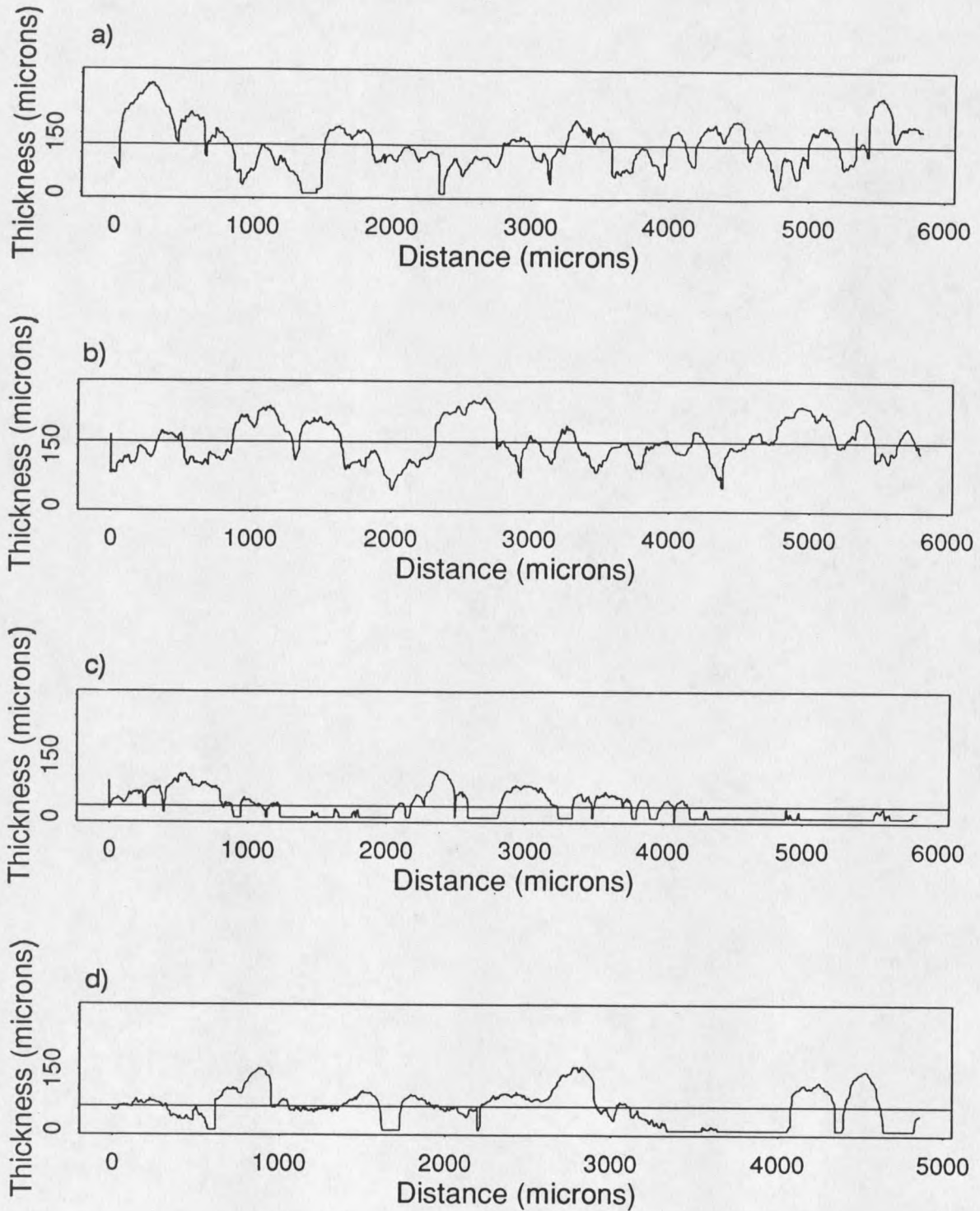


Figure 18. 4-day old binary population biofilm profiles a), b), c) and d) from different random locations on the slide.

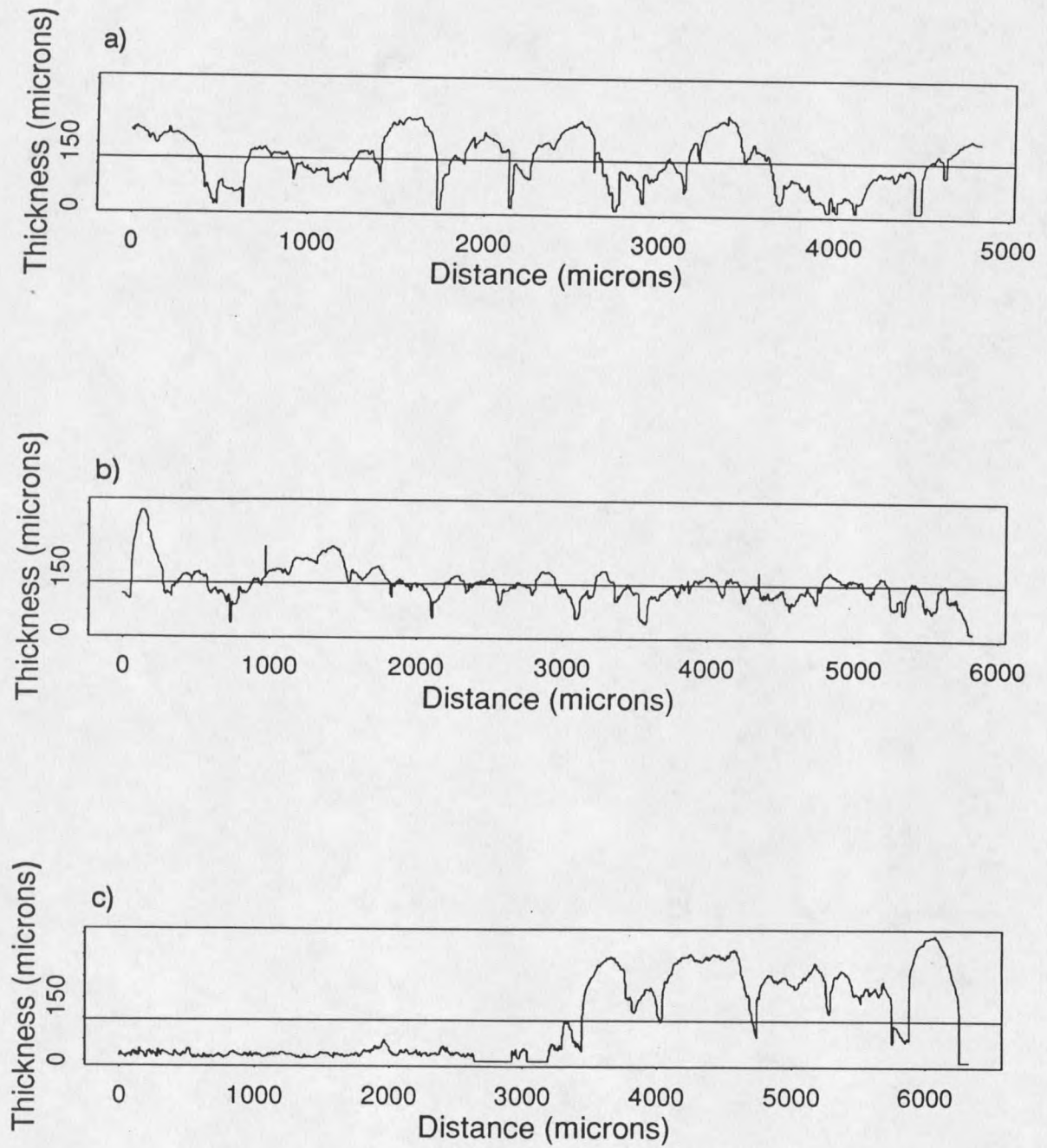


Figure 19. 6-day old binary population biofilm profiles a), b) and c) from different random locations on the slide.

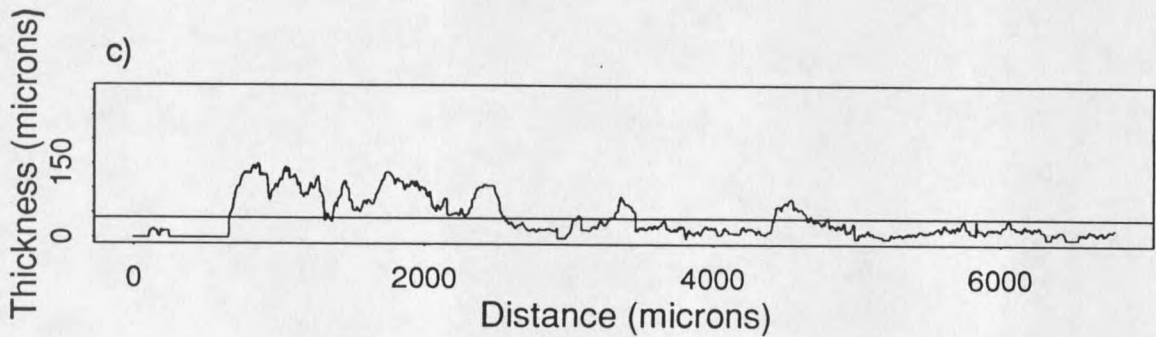
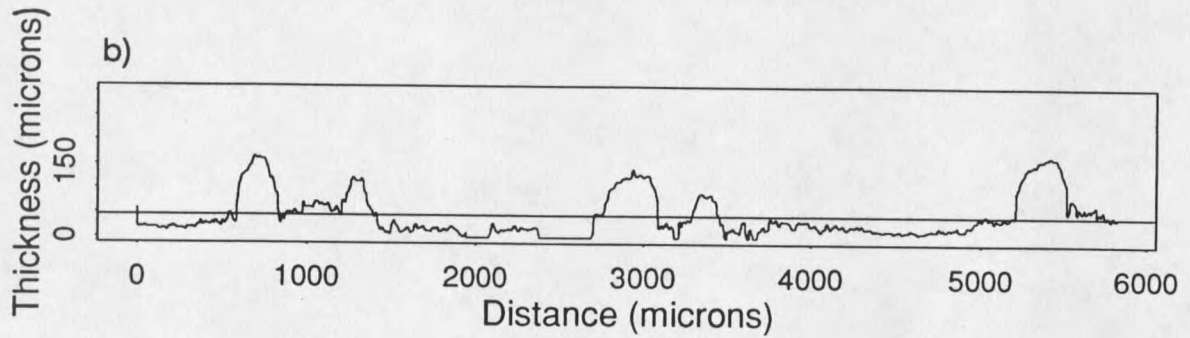
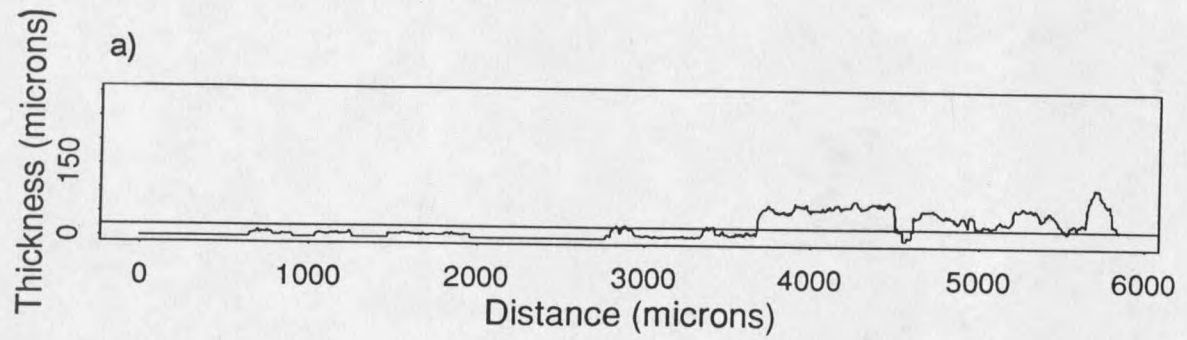


Figure 20. 8-day old binary population biofilm profiles a), b) and c) from different random locations on the slide.

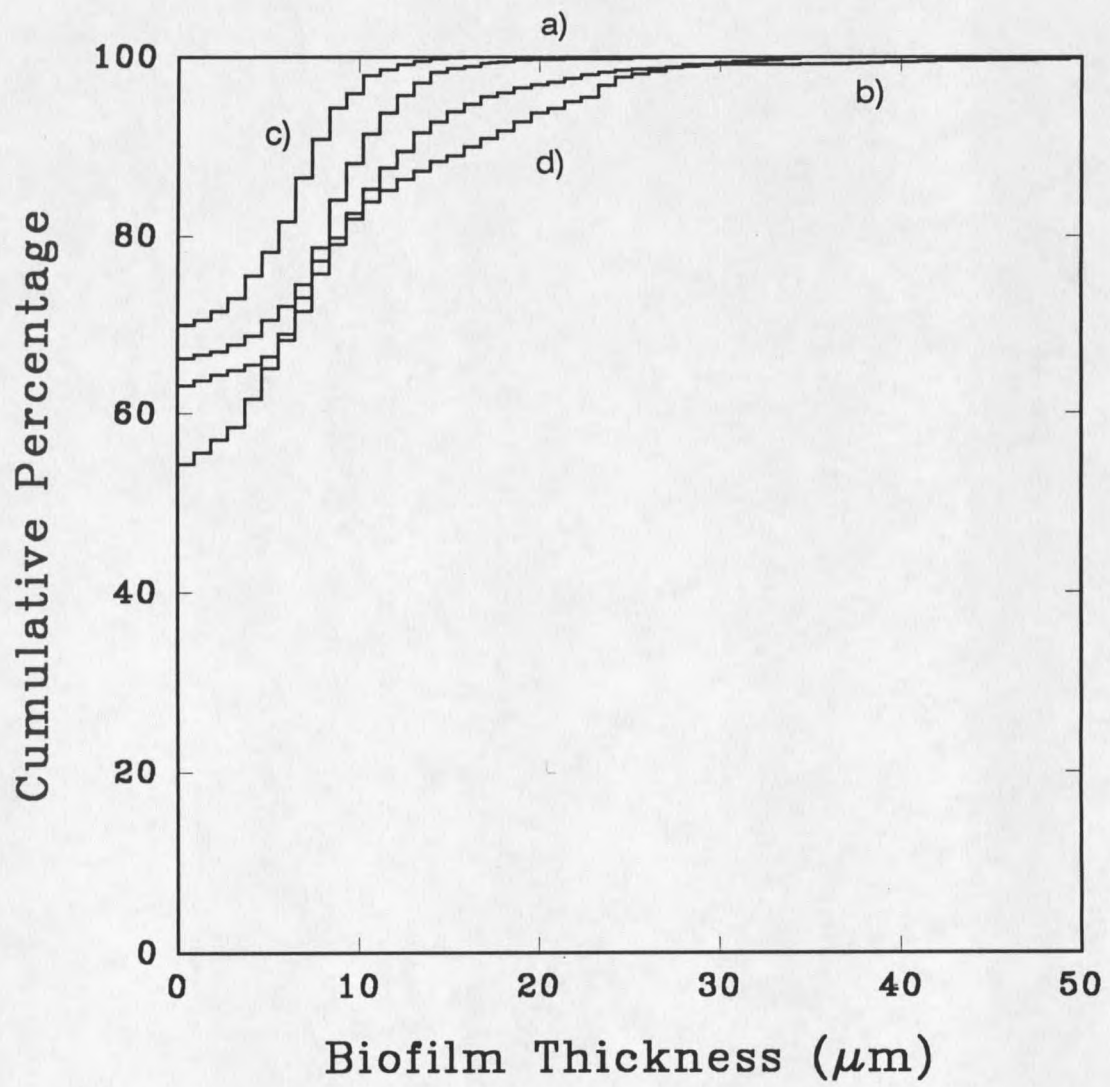


Figure 21. Binary population biofilm thickness distributions a), b), c) and d) from profiles on Figures 17a through 17d.

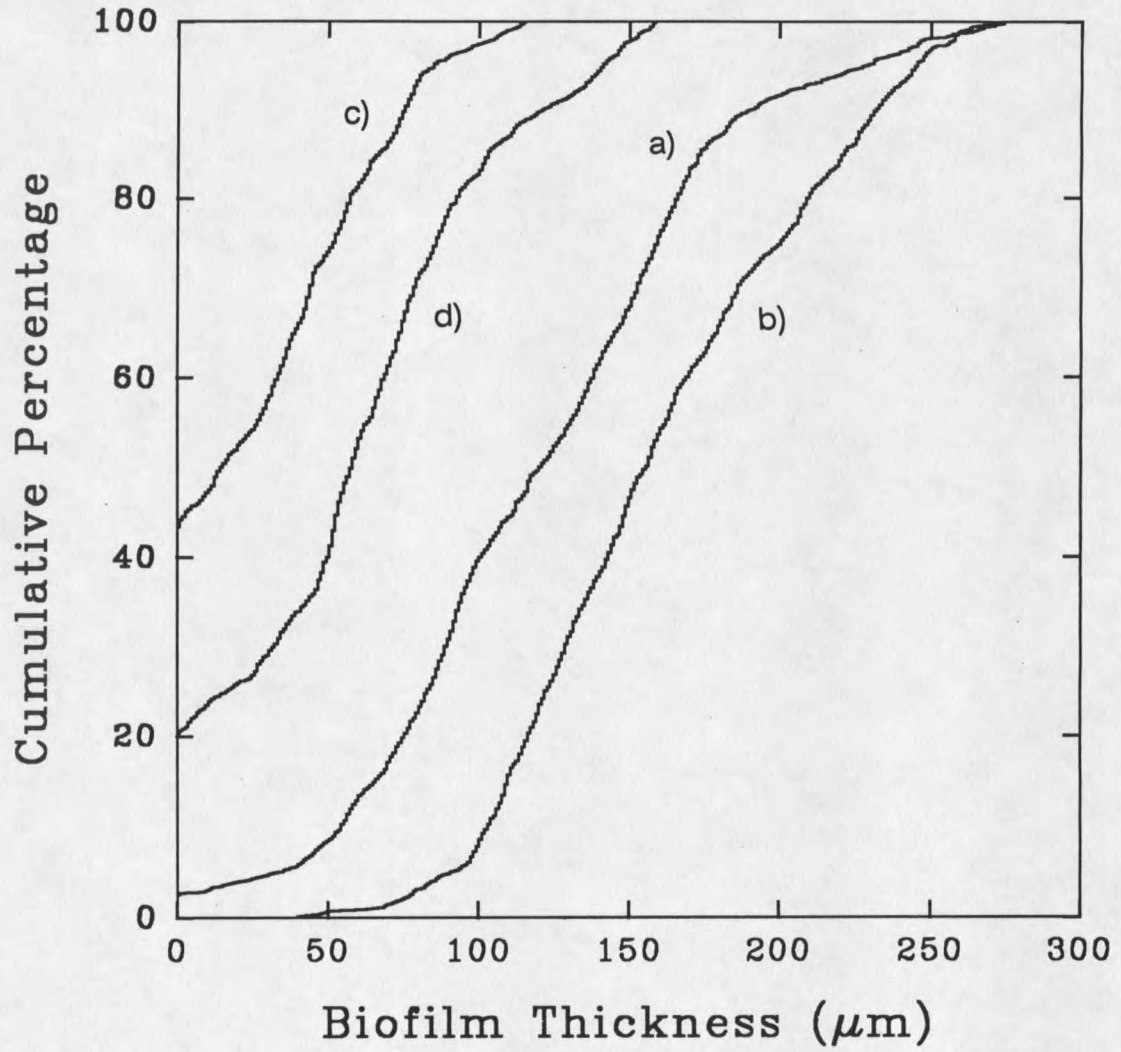


Figure 22. Binary population biofilm thickness distributions a), b), c) and d) from profiles on Figures 18a through 18d.

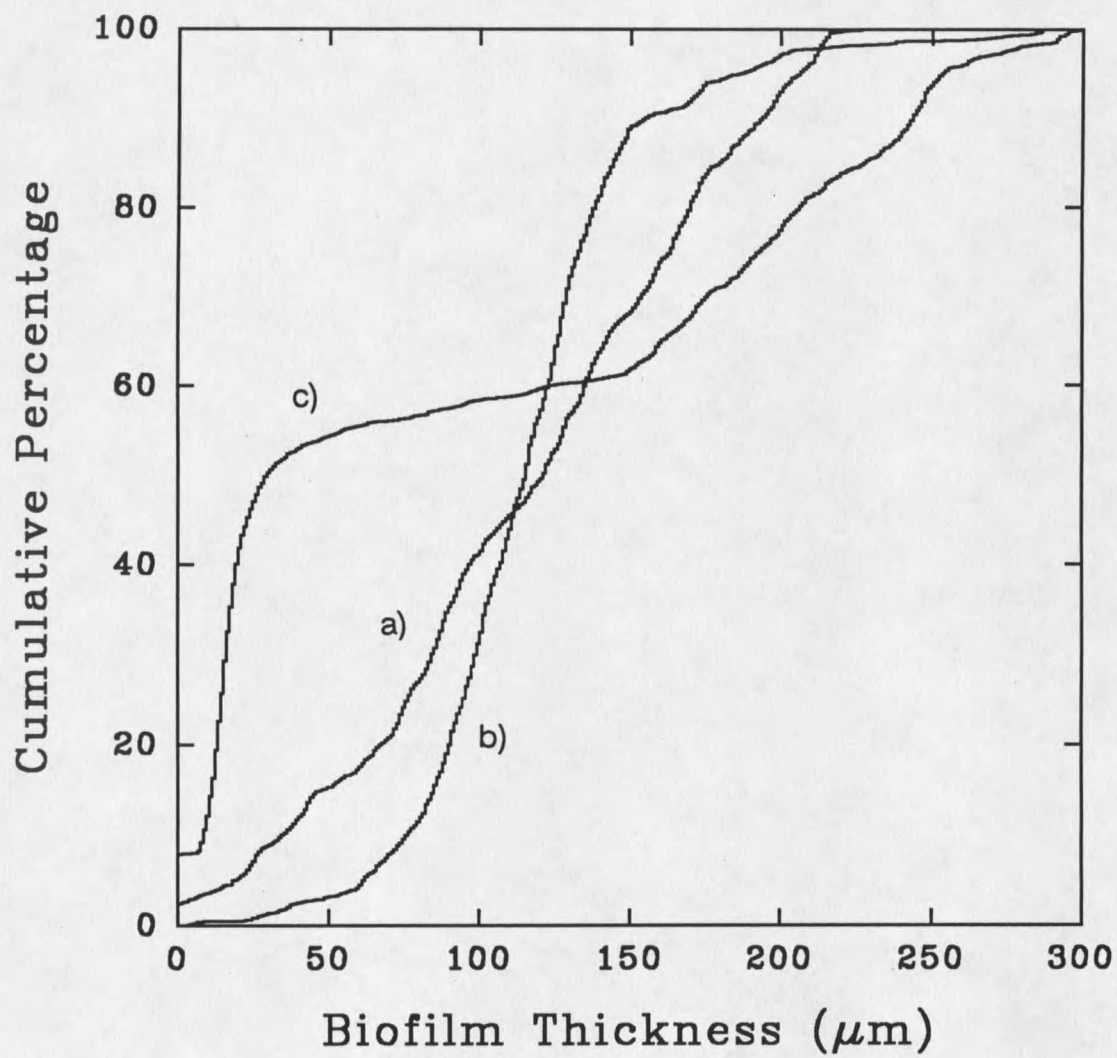


Figure 23. Binary population biofilm thickness distributions a), b) and c) from profiles on Figures 19a through 19c.

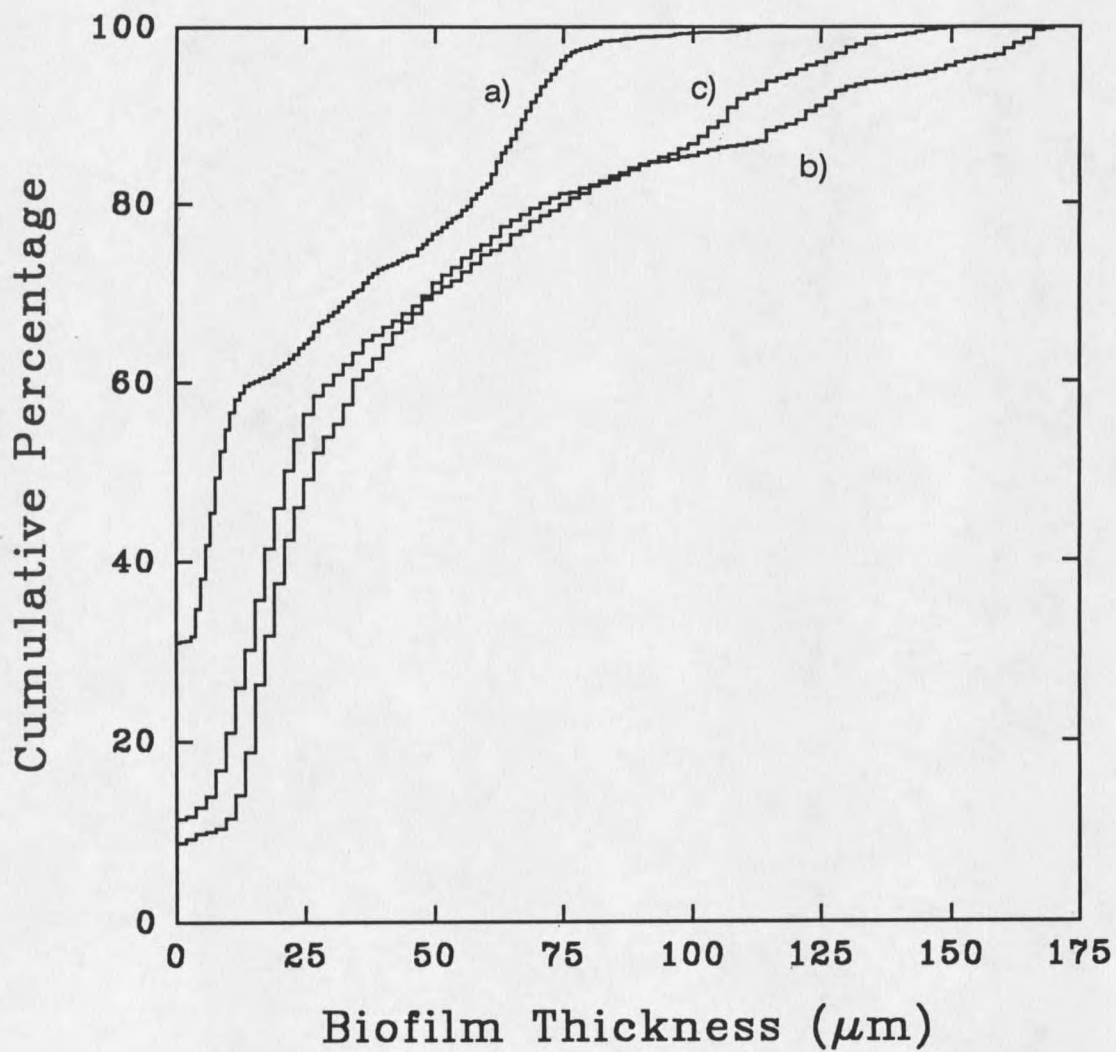


Figure 24. Binary population biofilm thickness distributions a), b) and c) from profiles on Figures 20a through 20c.

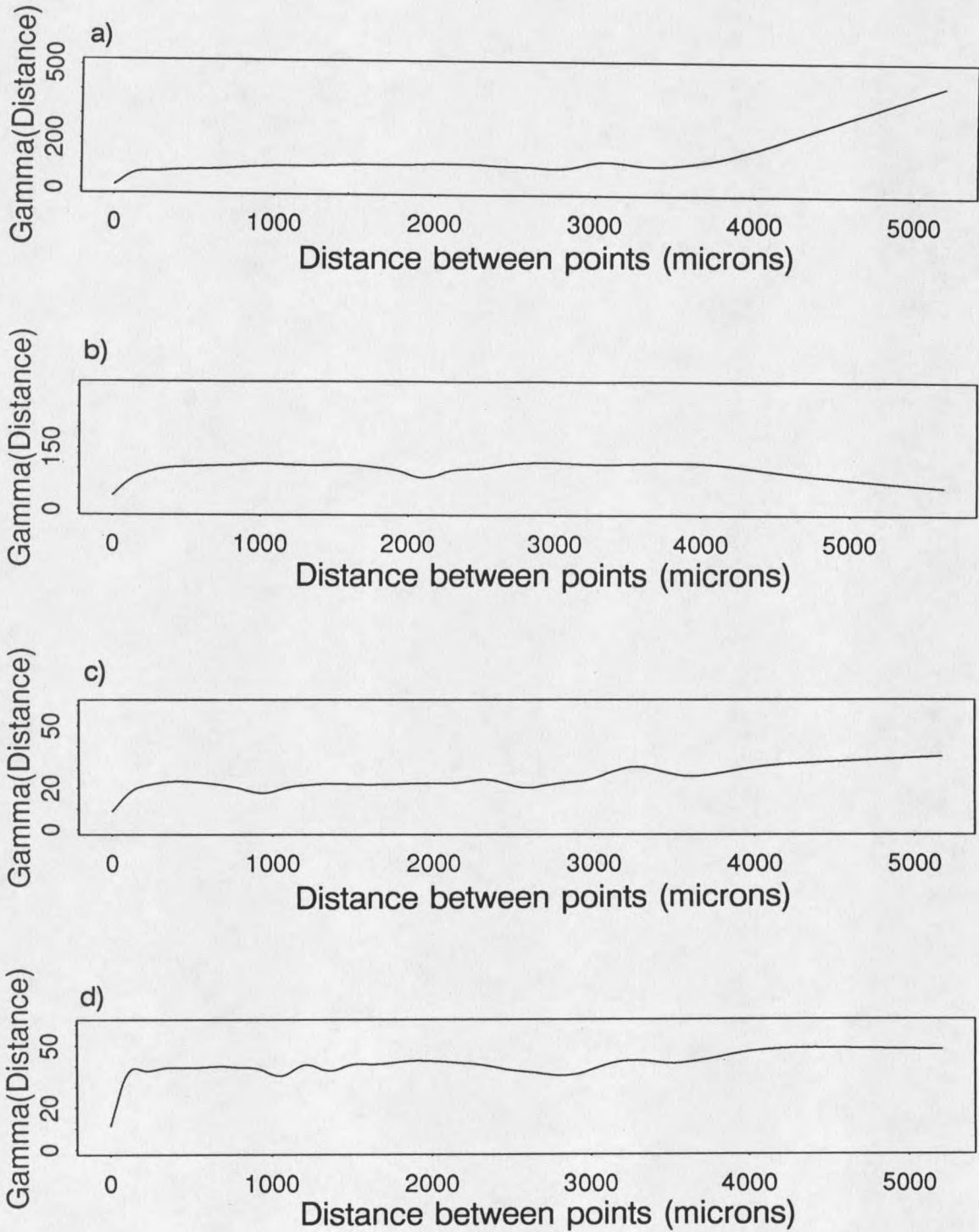


Figure 25. Variogram curves a), b), c) and d) from profiles on Figures 17a through 17d.

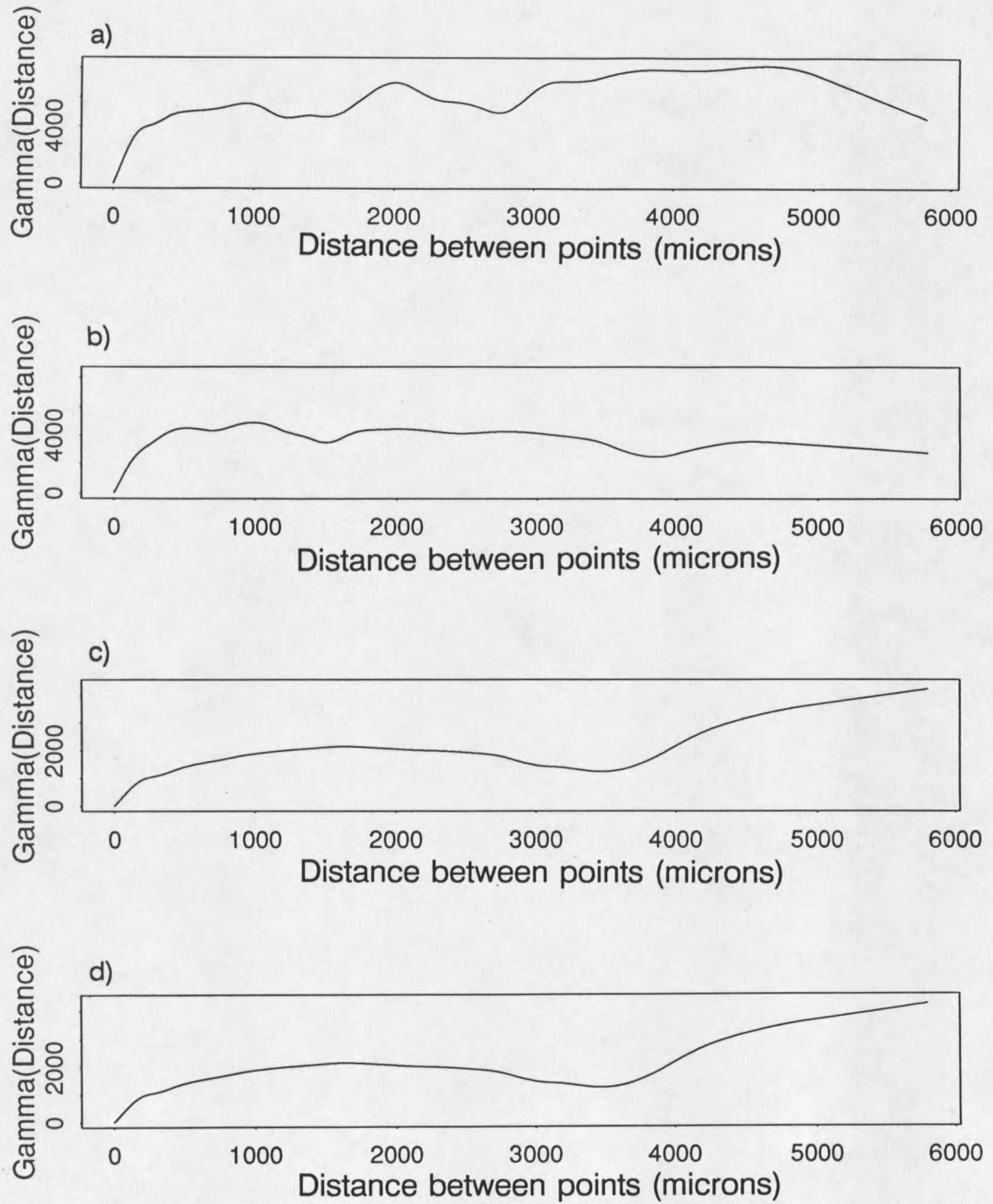


Figure 26. Variogram curves a), b), c) and d) from profiles on Figures 18a through 18d.

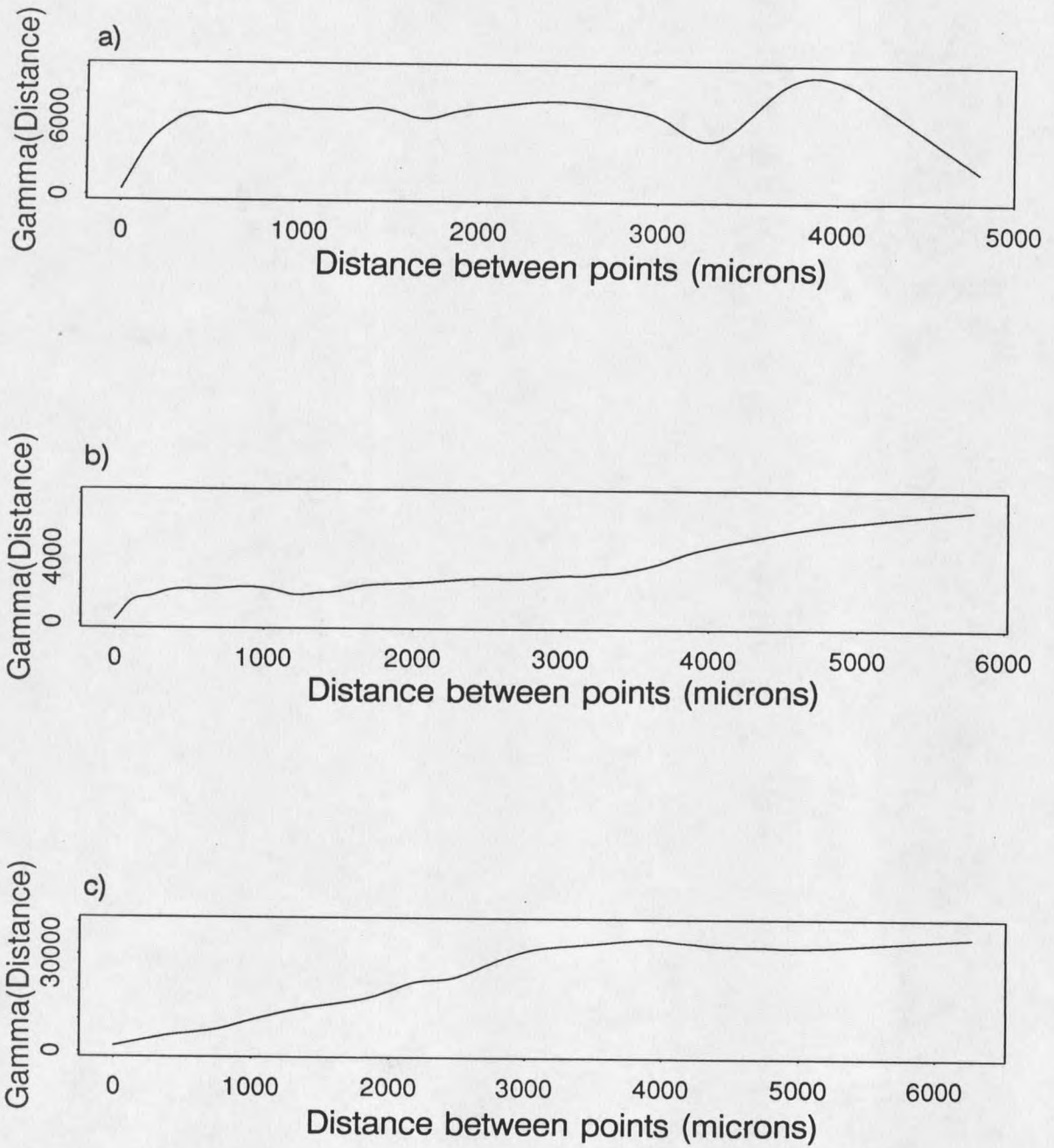


Figure 27. Variogram curves a), b) and c) from profiles on Figures 19a through 19c.

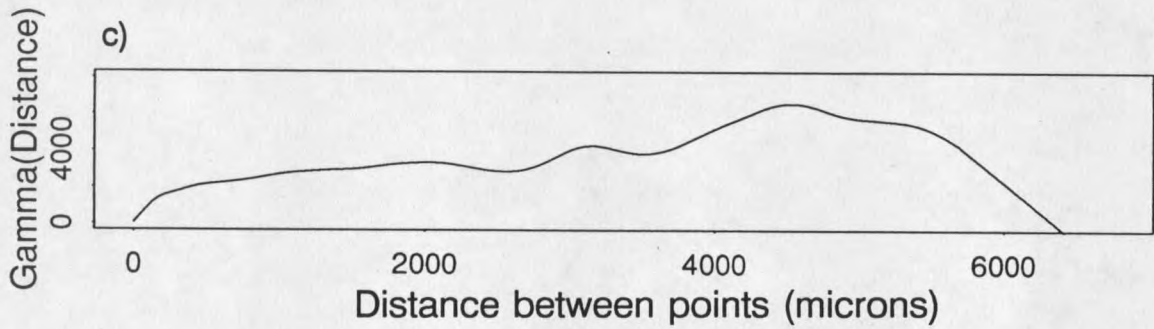
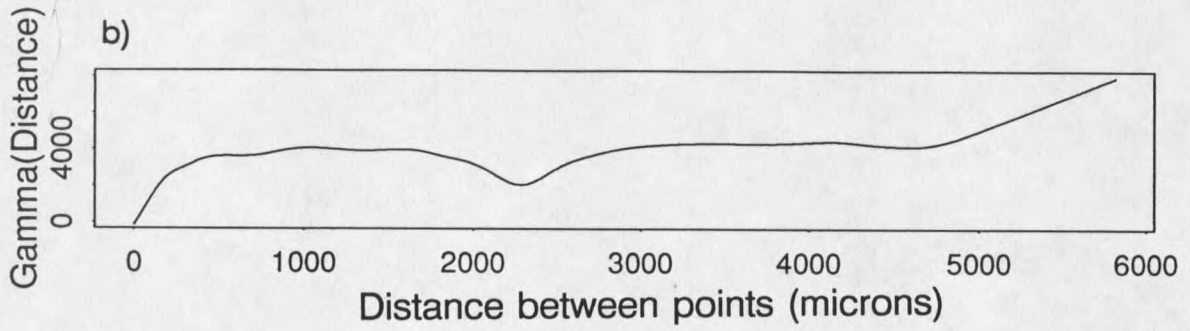
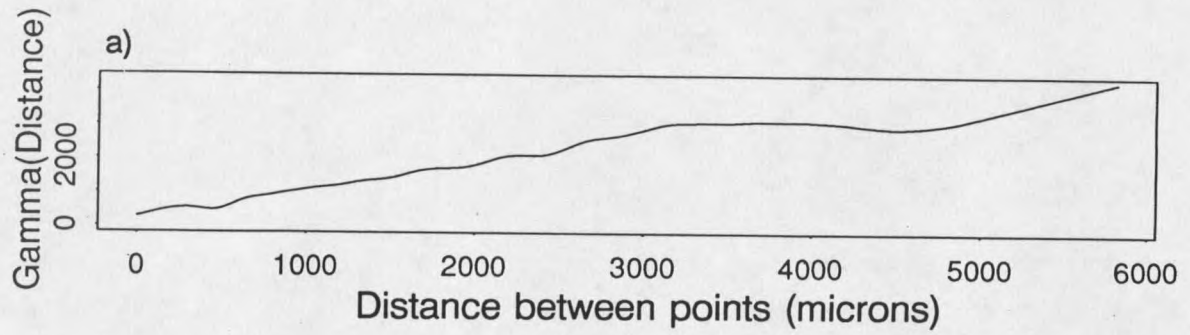


Figure 28. Variogram curves a), b) and c) from profiles on Figures 20a through 20c.

